Accepted Manuscript

Deletion of Endothelial TGF-β Signaling Leads to Choroidal Neovascularization

Anja Schlecht, Sarah V. Leimbeck, Herbert Jägle, Annette Feuchtinger, Ernst R. Tamm, Barbara M. Braunger

PII: S0002-9440(17)30415-7

DOI: 10.1016/j.ajpath.2017.06.018

Reference: AJPA 2699

To appear in: *The American Journal of Pathology*

Received Date: 0002-9440 February 0002-9440

Revised Date: 0002-9440 February 0002-9440

Accepted Date: 29 June 2017

Please cite this article as: Schlecht A, Leimbeck SV, Jägle H, Feuchtinger A, Tamm ER, Braunger BM, Deletion of Endothelial TGF-β Signaling Leads to Choroidal Neovascularization, *The American Journal of Pathology* (2017), doi: 10.1016/j.ajpath.2017.06.018.

Deletion of endothelial TGF-β signaling leads to choroidal neovascularization

Anja Schlecht[1], Sarah V. Leimbeck[1], Herbert Jägle[2], Annette Feuchtinger[3], Ernst R. Tamm[1]* and Barbara M. Braunger[1]*

[1] Institute of Human Anatomy and Embryology, University of Regensburg, Germany

[2] Department of Ophthalmology, University Clinic Regensburg, Germany

[3] Research Unit Analytical Pathology Helmholtz Zentrum München, Germany

* To whom correspondence should be addressed:

Barbara M. Braunger and Ernst R. Tamm, Institute of Human Anatomy and Embryology, University of Regensburg, Universitätsstr. 31, D-93053 Regensburg, Germany.

Tel.: +49-941/943-2812/-2839, E-mail: Barbara.Braunger@ur.de, Ernst.Tamm@ur.de

Running title: TGF-β and choroidal neovascularization

Financial Support/Sources of Funding: Deutsche Forschungsgemeinschaft FOR 1075 and TP5 (E.R.T.)

Disclosures: None declared.

Abstract

The molecular pathogenesis of choroidal neovascularization (CNV), an angiogenic process that critically contributes to vision loss in age-related macular degeneration (AMD) is unclear. Here we analyzed the role of transforming growth factor (TGF)-β signaling for CNV formation by generating a series of mutant mouse models with induced conditional deletion of TGF-β signaling in the entire eye, the retinal pigment epithelium (RPE) or the vascular endothelium. Deletion of TGF-β signaling in the eye caused CNV, irrespectively if it was ablated in newborn or three-week-old mice. Areas of CNV showed photoreceptor degeneration, multilayered RPE, basal lamina deposits and accumulations of monocytes/macrophages. The changes progressed leading to marked structural and functional alterations of the retina. While the specific deletion of TGF-β signaling in the RPE caused no obvious changes, specific deletion in vascular endothelial cells caused CNV and a phenotype quite similar to that observed after the deletion in the entire eye. We conclude that impairment of TGF-β signaling in the vascular endothelium of the eye is sufficient to trigger CNV formation. Our findings highlight the importance of TGF-β signaling as key player in the development of ocular neovascularization and indicate a fundamental role of TGF-β signaling in the pathogenesis of AMD.

Key words: TGF-β signaling; RPE; retina; angiogenesis; vascular endothelium

Introduction

The therapeutic options to treat age-related macular degeneration (AMD), the leading cause of vision loss and blindness in industrialized countries,[1–3] are limited.[4,5] AMD is a complex disease[6] whose molecular pathogenesis is not well understood.[4,5] Vision loss in AMD is caused by choroidal neovascularization (CNV) or geographic atrophy.[4,5,7] In geographic atrophy ("late dry" AMD), the progressive atrophy of the retinal pigment epithelium (RPE) and of the choriocapillaris are likely causes of photoreceptor degeneration.[5] Angiogenic processes that cause immature choroidal vessels to break in and through the RPE into the subretinal space characterize CNV.[8] The resulting blood and plasma leakage causes fibrous scarring of the retina ("wet" AMD). The pathogenic mechanisms underlying the onset of CNV in AMD are unclear. Dysfunction of the retinal pigment epithelium (RPE) and a dysregulation of pro-angiogenic and immune-stimulating molecular factors in the region of the retinal/choroidal interface are considered as contributing factors.[4,7,9,10]

The choroidal vasculature forms the choriocapillaris, a vascular bed of highly anastomosed capillaries that is essential for nutrition and oxygen supply of both photoreceptors and RPE.[11] The capillaries have a fenestrated endothelial layer and are highly permeable,[12] a substantial difference to retinal capillaries. There is evidence from several studies of genetically engineered mouse models indicating that RPE-derived vascular endothelial growth factor (VEGF) is essential for choriocapillaris maintenance. VEGF is expressed in high amounts by RPE cells during embryonic development and in adult life.[13] If VEGF expression is compromised, formation of the choriocapillaris in development or its maintenance in adult eyes are severely impaired leading to choriocapillaris ablation.[14–18] Other growth factors that are secreted by RPE cells in high amounts are transforming growth factor (TGF)-β1 and –β2[19] causing a concentration of both factors in the RPE/choroid complex that is more than 10-fold higher than in the retina.[20] In a recent study we showed that a conditional ocular deletion of TGF-β signaling results in pronounced structural changes of retinal capillaries including the formation of abundant

76 microaneurysms, leaky capillaries, and retinal hemorrhages. Overall a phenotype resulted
77 very similar to that of diabetic retinopathy in humans.[21]

78 Since TGF-βs are present at very high concentrations in region of the RPE/choroid
79 interface, we wondered if TGF-β signaling might not only be required for stability of retinal
80 capillaries, but also for that of the choriocapillaris. To this end, we targeted the TGF-β type II
81 receptor (TβRII), which is essential for TGF-β signaling and generated a series of mutant
82 mouse strains with an induced conditional deletion in the entire eye, the RPE or in vascular
83 endothelial cells. Here we provide evidence that impairment of TGF-β signaling in the
84 vascular endothelium of the eye is sufficient for the development of CNV. Our findings
85 highlight the importance of the TGF-β signaling pathway as a key player in the development
86 of ocular neovascularization and indicate a fundamental role of TGF-β signaling in the
87 pathogenesis of AMD.

88

89

Material and Methods

Mice

All experiments were performed in mice of either sex that were tested negatively for the *Rd8* mutation.[22] Mice with two floxed alleles of *Tgfbr2* (*Tgfbr2*$^{fl/fl}$)[23] were crossed with heterozygous *CAGGCre-ER*^{TM},[24] *VMD2*^{rtTA}*-Cre*[25] or *VECad-Cre-ER*^{T2} [26] mice. Resulting *Tgfbr2*$^{fl/fl}$;*CAGGCre-ER*^{TM}, *Tgfbr2*$^{fl/fl}$;*VMD2*^{rtTA}*-Cre* or *Tgfbr2*$^{fl/fl}$;*VECad-Cre-ER*^{T2} mice were used as experimental mice. For simplicity, *Tgfbr2*$^{fl/fl}$;*CAGGCre-ER*^{TM} mice will be referred to as *Tgfbr2*$^{\Delta eye}$, *Tgfbr2*$^{fl/fl}$;*VMD2*^{rtTA}*-Cre* mice will be referred to as *Tgfbr2*$^{\Delta RPE}$ and *Tgfbr2*$^{fl/fl}$;*VECad-Cre-ER*^{T2} mice will be referred to as *Tgfbr2*$^{\Delta EC}$. *Tgfbr2*$^{fl/fl}$ littermates with two unrecombined *Tgfbr2* alleles served and are referred to as controls. Genetic backgrounds were 129SV (*Tgfbr2*$^{fl/fl}$, *VMD2*^{rtTA}*-Cre, VECad-Cre-ER*^{T2}) and C57/Bl6 (*CAGGCre-ER*^{TM}). All mice were reared in a light/dark cycle of 12 h (lights on at 7 AM). Genotypes were identified by isolating genomic DNA from tail biopsies, and testing for transgenic Cre sequences and floxed *Tgfbr2* sequences as described previously.[21,27]

Induction of Cre recombinase

Cre recombinase in *CAGGCre-ER*^{TM} and *VECad-Cre-ER*^{T2} mice is tamoxifen dependent. In *CAGGCre-ER*^{TM} mice, the *Cre-ER*^{TM} fusion protein is ubiquitously expressed. Cre recombinase is restricted to the cytoplasm and will only access the nucleus after binding to tamoxifen.[24,28] *VECad-Cre-ER*^{T2} mice carry the Cre-ER^{T2} expression cassette under regulatory control of the mouse VE-cadherin gene promoter region that specifically drives gene expression in the vascular endothelium.[26] To activate Cre recombinase in *Tgfbr2*$^{\Delta eye}$ and*Tgfbr2*$^{\Delta EC}$ mice, the conditional knockout animals and their respective control littermates were equally treated with tamoxifen containing eye drops from postnatal day (P) 4 to P8 as described previously.[29] A second stock of *Tgfbr2*$^{\Delta eye}$ and control mice was treated from P21 to P25, a time when the development of the retinal vasculature is complete. For simplicity, *Tgfbr2*$^{\Delta eye}$ mice that were tamoxifen treated from P4-8 will be referred to as “early-induced” and *Tgfbr2*$^{\Delta eye}$ mice that were tamoxifen treated from P21-25 will be referred to as “late-

induced". Cre recombinase in *VMD2^{rtTA}-Cre*;*Tgfbr2$^{fl/fl}$* is doxycycline dependent and under the control of the RPE-specific bestrophin promotor.[25] Doxycycline (AppliChem, Darmstadt, Germany) was diluted in phosphate-buffered saline (PBS) to a final concentration of 0.1 g/ml and doxycycline eye drops (10 µl) were pipetted onto the eyes of *Tgfbr2$^{\Delta RPE}$* mice and their control littermates from P21 to P25 three times per day. We provide a detailed list of the individual treatment time points and subsequently performed analyses of the eyes in table 1.

mT/mG and *R26R* reporter mice

The efficiency of the Cre recombinase activation in *VeCad-Cre-ER^{T2}* mice was confirmed using *mT/mG* reporter mice,[30] which express a membrane-targeted green fluorescent protein (mG/GFP) after Cre mediated excision. Heterozygous *VeCad Cre-ER^{T2}* mice were crossed with homozygous *mT/mG* mice. The resulting offspring (*VeCad-Cre-ER^{T2}(+/-) ;mT/mG(+/-)* and *wildtype;mT/mG(+/-)*) was treated with tamoxifen eyedrops from P4 to P8 according to previously published protocols.[21,29] Mice were killed at P10. After enucleation, the eyes were fixed in 4% paraformaldehyde (PFA) for 4 h, washed extensively in phosphate buffer (PB, 0.1 M, pH 7.4), incubated in 10%, 20%, 30% sucrose overnight and shock frozen in tissue-mounting medium (O.C.T. Compound; DiaTec, Bamberg, Germany). Frozen sections were washed three times in phosphate buffer (PB, 5 min each) and cell nuclei were counterstained with DAPI (Vectashield; Vector Laboratories, Burlington, CA) 1:10 diluted in fluorescent mounting medium (Serva, Heidelberg, Germany). Successful activation of the Cre recombinase in *CAGG-Cre-ER^{TM}* mice was confirmed using *R26R* reporter mice.[31] Heterozygous *CAGGCre-ER^{TM}* mice were crossed with homozygous *R26R* mice. The resulting offspring was treated with tamoxifen eye drops from P21 to P25 according to previously published protocols. [27,29] Mice were killed at the age of four weeks, the eyes were enucleated and processed for LacZ-staining which was performed as described previously.[29,32] Paraffin sections were analyzed by light microscopy (Carl Zeiss, Jena, Germany).

Tgfbr2 deletion PCR

Tgfbr2 deletion PCR screens its successful genomic deletion following Cre mediated recombination. DNA samples of the sensory retina and the choroid (including cells of the RPE) served as templates. Primer pairs and protocols are described elsewhere.[29,33] Actin was used as the loading control.

Morphology and microscopy

Eyes were enucleated, fixed for 24 h in 2% PFA/2.5% glutaraldehyde[34] and embedded in Epon (Serva, Heidelberg, Germany) as described elsewhere.[35,36] Semithin meridional sections (1 µm thick) were cut through the eyes and stained after Richardson.[37] The sections were analyzed on an Axio Imager Z1 microscope (Carl Zeiss) using Axiovision version 4.8 software (Carl Zeiss). Ultrathin sections were processed according to protocols published previously,[38,39] stained with uranyl acetate and lead citrate, and analyzed on a transmission electron microscope (Libra, Zeiss).

Immunohistochemistry

Prior to TβRII, collagen IV and VEGF-A staining, eyes were fixed for 4 h in 4% PFA, washed extensively in PB (0.1 M, pH 7.4) and embedded in paraffin according to standard protocols. Paraffin sections (6 µm) were deparaffinized and washed in H_2O. For detection of TβRII, sections were treated with boiling citrate buffer (1 x 10 min, pH 6), washed again in H_2O and incubated in PB. For detection of collagen IV and VEGF-A, sections were pretreated with 0.05 M Tris-HCl (5 min) and covered with Proteinase K (100 µl of Proteinase K in 57 ml of Tris-HCl (0.05 M), 5 min), washed in H_2O, incubated in 2 N HCl (20 min), and washed again in H_2O. Sections were incubated in PB for 5 min and then blocked with 2% BSA, 0.2% CWFG, 0.1% Triton X (TβRII), 2% BSA, 0.1% Triton X (Collagen IV) or 5% non-fat dry milk (VEGF-A) at room temperature for 60 min. Primary antibodies (Table 2) were diluted in a 1:10 dilution of blocking solution in PB. Prior to F4/80 and PLVAP staining, eyes were fixed for 4 h in 4% PFA, washed extensively in PB, incubated in 10%, 20%, 30% sucrose/PBS

overnight at 4 ℃ and shock frozen in tissue mounti ng medium. For immunohistochemistry, frozen sections were washed three times in PB or PBS (F4/80) for 5 min each and blocked at room temperature with 2% BSA in PB for 45 min (F4/80: 1% non-fat dry milk, 0.01% Tween in PB). Primary antibodies (Table 2) were diluted in a 1:10 dilution of blocking solution in PB (F4/80: 2% BSA, 0.02% NaN_3, 0.01% Triton X in PBS) and incubated at 4 ℃ over night. After three washes in PB/PBS (5 min each), biotinylated antibodies were applied for 1 h, diluted in a 1:10 dilution of the blocking solution, then appropriate secondary antibodies (Table 2), diluted in a 1:10 dilution of the blocking solution, were applied on the sections for 1 h. Sections were washed again three times in PB/PBS and cell nuclei were counterstained with DAPI (Vectashield, Vector Laboratories) diluted (1:10) in fluorescent mounting medium (Serva, Heidelberg, Germany). Sections were investigated on an Axio Imager Z1 fluorescent microscope (Carl Zeiss) using appropriate Axiovision version 4.8 software (Carl Zeiss).

Quantification of F4/80 positive cells on immunohistochemical sections

Experimenters were blinded regarding to the genotype. Antibody incubation times were strictly monitored and microscope settings, e.g. the illumination time and intensity, were identical between individual sections. Only sections in midsagittal orientation were analyzed that stretched through the optic nerve to ensure comparable situations between the individual sections. F4/80 positive cells were counted per hemisphere in the retina and in the choroid/choriocapillaris.

Dextran perfusion

Prior to dextran perfusion, mice were deeply anesthetized with ketamine (120 mg/kg body weight (bw)) and xylazine (8 mg/kg bw). Afterwards mice were perfused through the left ventricle with 1 ml of PBS containing 50 mg FITC-dextran (MW = 2000 kDa, TdB Consultancy, Uppsala, Sweden). The eyes were enucleated and fixed in 4% PFA for 2 h (flatmounts)/4 h (sections) and washed in PB. Eyes were sectioned, placed on glass slides and counterstained with DAPI (Vectashield, Vector Laboratories) 1:10 diluted in fluorescent

mounting medium. FITC-dextran perfused sections were investigated on an Axio Imager Z1 fluorescent microscope (Carl Zeiss).

Quantification of choroidal neovascularization

Following dextran perfusion, flatmounts of the posterior eye segment (containing the retina, RPE, choroid and sclera) were dissected. Similar to the preparation of retinal flatmounts, the posterior eye segment was flat mounted on glass slides using fluorescent mounting medium. The entire flatmount was analyzed using an Axio Imager Z1 fluorescent microscope. Focusing on the retinal pigment epithelium allowed the quantification of the CNV penetrating through the RPE. To visualize the CNV, Z-stacks were generated that ranged from the superficial retinal plexus to the optical barrier of the pigmented RPE.

Electroretinography (ERG)

Mice were dark adapted for at least 12 h before the experiments and anesthetized by s.c. injection of ketamine (65 mg/kg bw) and xylazine (13 mg/kg bw). Pupils were dilated with tropicamide eye drops (Mydriaticum Stulln; Pharma Stulln GmbH, Stulln, Germany). Silver needle electrodes served as reference (forehead) and ground (tail), and gold wire ring electrodes served as active electrodes. ERGs were recorded with a Ganzfeld bowl (Ganzfeld QC450 SCX, Roland Consult, Brandenburg, Germany) and an amplifier/recording unit (RETI-Port, Roland Consult), band-pass filtered (1 to 300 Hz), and averaged. Single-flash scotopic (dark adapted) responses to a series of 10 LED-flash intensities (range: -3.5 to 1.0 log cd.s/m^2) were recorded. After 10 min of adaption to a white background illumination (20 cd/m^2) single flash photopic (light adapted) responses to three Xenon-flash intensities (1, 1.5 and 2 log cds/m^2) were recorded. All analyses and plotting were performed with R version 3.2.1 (The R Foundation for Statistical Computing, Vienna, Austria) and ggplot2 version 2.1.0.[40]

Fundus Imaging and Angiography

Imaging of the retinal vasculature was performed with a commercially available imaging system (Micron III; Phoenix Research Laboratories, Pleasanton, CA). Light source and imaging path filters (low pass and high pass at 500 nm) were used for fluorescein angiography (FLA). Mice were anesthetized by s.c. injection of ketamine (65 mg/kg body weight (bw)) and xylazine (13 mg/kg bw), and their pupils were dilated with tropicamide eye drops before image acquisition. FLA was performed with s.c. injection of 75 mg/kg bw fluorescein-Na (Alcon, Hünenberg, Switzerland).

RNA Analysis

Total RNA from retinae was extracted with TriFast, and first-strand cDNA synthesis was performed with iScript cDNA Synthesis Kit (Bio-Rad Laboratories, Inc., Hercules, CA) according to the manufacturer's guidelines. Quantitative real time RT-PCR analyses were performed with the iQ5 Realtime PCR Detection System (Bio-Rad Laboratories, Inc.). The temperature profile was denaturation at 95℃ for 10 s and annealing and extension at 60℃ for 40 s for 40 cycles. All primer pairs were purchased from Invitrogen and extended over exon-intron boundaries, except for *Gapdh*. Sequences of primer pairs are shown in Table 3. RNA that was not reverse transcribed served as a negative control for real time RT-PCR. Before relative quantification, mRNAs from three different potential housekeeping genes were tested: glyceraldehyde 3-phosphate dehydrogenase (Gapdh), guanine nucleotide binding protein (Gnb2l) and ribosomal protein L32 (Rpl32). We performed statistical analyses to confirm that none of the housekeeping genes were regulated and then used the geometric mean of the crossing thresholds of all three housekeeping genes for relative quantification. Quantification was performed using BioRad iQ5 Standard-Edition (Version 2.1) software (Bio-Rad Laboratories GmbH, Munich, Germany) and the ΔΔCt method in Excel (Microsoft Corporation, Redmond, WA, USA).[41]

Deep tissue imaging by 3D light-sheet fluorescence microscopy

Mice were deeply anesthetized with ketamine (120 mg/kg bw) and xylazine (8 mg/kg bw) and 130 µl of *Tomato lectin* (Perkin Elmer, Inc., Waltham, MA) were injected slowly intravenously. Mice were killed 15 min after injection by cervical dislocation. The eyes were enucleated and fixed using Paxgene Tissue Containers (Qiagen, Hilden, Germany) according to the manufacturer's recommendations and thereafter underwent a chemical procedure of optical clearing as previously described.[42] Cleared transparent whole mouse eyes were imaged on a light-sheet fluorescence microscope (UltraMicroscope II, LaVision BioTec, Bielefeld, Germany), equipped with a sCMOS camera (Andor Neo, Concord, USA) and a 2x/0.5 NA objective lens (MVPLAPO 2x, Olympus, Hamburg, Germany). The specimens were two-sided illuminated by a planar light-sheet using a white light laser (SuperK EXTREME EXW-9, NKT Photonics, Birkeröd, Denmark). To visualize the specific TLectinSense680 signals for vascularization, a bandpass filter set with an excitation range of 640/30 and emission range of 690/50 was used in combination with an additional filter set (excitation: 531/40; emission: 593/40) for detection of autofluorescence (morphology). By moving the specimen chamber vertically stepwise (step-size 4 µm) through the laser light-sheet, optical sections were obtained. In order to ensure standardized imaging regions for each eye the scan always covered 600 µm above to 600 µm below the optical nerve. Maximum intensity projections were performed by ImspectorPro Software (LaVision BioTec, Bielefeld, Germany).

Statistical Analysis

All results are expressed as means ± SEM. Comparisons between the mean variables of two groups were made by a two-tailed Student's *t*-test. Significance of the ERG analyses was evaluated using a one-way ANOVA test, followed by Tukey HSD post hoc test. $P \leq 0.05$ was considered to be statistically significant.

282 Study approval

283 All procedures conformed to the tenets of the NIH's Guidelines for the Care and Use of
284 Laboratory Animals, the EU Directive 2010/63/E, institutional guidelines, and were approved
285 by the local authority (Regierung der Oberpfalz, AZ 54-2532.1-44/12 and DMS 2532-2-85).

286

287

Results

Deletion of ocular TGF-β signaling in mouse pups leads to choroidal neovascularization

To investigate the role of the TGF-β signaling pathway for the structure of retinal and choroidal vessels, we deleted the essential TβRII receptor in the eyes via tamoxifen-induced conditional deletion. To this end, *Tgfbr2fl/fl;CAGGCre-ER^{TM}* mice were generated and treated from postnatal day (P) 4 to P8 with tamoxifen eye drops. For simplicity we will refer to *Tgfbr2fl/fl;CAGGCre-ER^{TM}* mice that received tamoxifen by this protocol as early-induced *Tgfbr2$^{\Delta eye}$* mice and tamoxifen-treated littermates with two unrecombined *Tgfbr2$^{fl/fl}$* alleles are referred to as controls. As shown previously, the treatment results in a significant reduction of TβRII and its mRNA in the eyes of early-induced *Tgfbr2$^{\Delta eye}$* mice compared to controls [21]. We also observed in the previous study that the deletion of ocular TGF-β signaling leads to the formation of abundant microaneurysms in retinal vessels and to a phenotype that largely mimics that of nonproliferative and proliferative diabetic retinopathy in humans.[21] Consequently we observed in the retina of two- and three-month-old early-induced *Tgfbr2$^{\Delta eye}$* mice vascular microaneurysms in the inner nuclear layer, which were characterized by their large lumen and thick coat of endothelial cells (Fig. 1A, B, C). In contrast, no changes were seen in control mice (Fig. 1A and B). We now turned our attention to the choroidal/retinal interface that we had not analyzed previously. Here we frequently observed focal areas in which the outer segments of photoreceptors were completely missing and the thickness of the outer nuclear layer was substantially reduced (Fig. 1B and C). Accumulations of cells were present between photoreceptors and RPE. The cells frequently surrounded vascular openings filled with erythrocytes strongly indicating their endothelial origin and an ongoing neoangiogenetic process. The RPE was multilayered in those areas, and contained cystic and amorphous inclusions (Fig. 1C). When investigating serial sections we observed vessels beneath and above the RPE, concomitant with type 1 (sub-RPE, occult) and type 2 (sub-retinal, classic) CNV in human patients.

To characterize the origin of the newly formed vessels in the subretinal space (between the sensory retina and the RPE) of early-induced *Tgfbr2$^{\Delta eye}$* mice, we now perfused the mice with

high molecular weight FITC-dextran for vascular labeling. While the retinal and choroidal vasculature of control animals was essentially normal, distinct changes were observed in the subretinal space of early-induced *Tgfbr2*$^{\Delta eye}$ mice. Here we observed vessels breaking from the choroid through Bruch's membrane (BM) across the RPE into the subretinal space (Fig. 2A). FITC dextran-perfused flat mounted posterior eye segments (containing the retina, RPE, choroid and sclera) of four- to six-week-old animals had 2.86 ± 0.59 CNV per eye (n = 7, supplemental Fig. 1B). To confirm this observation by an independent method, we next performed 3D imaging of lectin perfused, optical cleared and transparent whole eyes (Fig. 2B). The choriocapillaris did not resolve into single capillaries but rather appeared as an intense fluorescent line covering the outer surface of the retina, a fact that we attributed to the immense density and blood flow of this capillary bed.[43] In control eyes, the three plexus of the retinal vasculature could be completely visualized and were essentially normal. In contrast, in early-induced *Tgfbr2*$^{\Delta eye}$ mice, vessels that originated from the choriocapillaris entered the retina and continued into the retinal vascular bed forming obvious anastomoses with retinal vessels (Fig. 2B). We now characterized the vascular wall of the newly formed vessels by transmission electron microscopy (TEM). As expected, in control mice the endothelium surrounding retinal vessels was continuous (Fig. 2C) while that around the choriocapillaris was fenestrated. When we analyzed the newly formed vessels in the subretinal space of early-induced *Tgfbr2*$^{\Delta eye}$ mice, distinct fenestrations covered by a typical diaphragm were regularly observed (Fig. 2C). To further support this finding, we performed immunohistochemical staining for plasmalemma vesicle-associated protein (PLVAP), a vascular protein, intrinsic component of the diaphragm of vascular fenestrae, and marker for fenestrated endothelia.[44–47] As expected, in control and early-induced *Tgfbr2*$^{\Delta eye}$ animals the continuous endothelium of the retinal vasculature did not show any PLVAP immunoreactivity (supplemental Fig. 1A) while the fenestrated endothelium of the choriocapillaris showed an intense PLVAP signal (Fig. 2D). In early-induced *Tgfbr2*$^{\Delta eye}$ mice though, intense PLVAP immunoreactivity was observed in the areas of neovascularization in the subretinal space

(Fig. 2D). Overall our results strongly indicated that loss of TGF-β signaling in early-induced *Tgfbr2*$^{\Delta eye}$ mice caused choroidal neovascularization (CNV).

TGF-β signaling is required to prevent choroidal neovascularization in late-induced *Tgfbr2*$^{\Delta eye}$ mice

Next we wondered whether the formation of CNV after TβRII deletion might be supported by the fact that retinal vascular development is not completed in mouse pups and signaling processes are continuously ongoing that promote angiogenesis. To learn if TGFβ-signaling is also important for maintenance of the adult choriocapillaris when retinal vascular development is completed, we deleted TGFβ-signaling by an essentially comparable approach in three-week-old mice with completely developed retinal vasculature. Mice were treated with tamoxifen eye drops from P21 – P25 and are further referred to as late-induced *Tgfbr2*$^{\Delta eye}$ mice. To confirm successful tamoxifen-induced recombination, we crossed the mice with Cre reporter mice carrying the Rosa26 reporter (*R26R*) allele. Tamoxifen-treated eyes were stained for β-galactosidase and an intense staining was seen throughout the eye of *CAGGCre-ER*^{TM};*R26R* mice, whereas ocular tissues of *R26R* littermates, which did not carry the *CAGGCre-ER*^{TM} transgene, were completely unstained (supplemental Fig. 2A). Furthermore, the significant deletion of retinal *Tgfbr2* was confirmed by real time RT-PCR analyses (Supplemental Fig. 2B). Next, we analyzed the ocular morphology of late-induced *Tgfbr2*$^{\Delta eye}$ mice and controls at the age of three (Fig. 3A and B) and six months (Fig. 4A and C). Retinal structure was essentially normal in control animals (Fig. 3A, B and Fig. 4A, C) and no obvious changes were observed in the inner retina of three-month-old late-induced *Tgfbr2*$^{\Delta eye}$ animals (Fig. 3B). However, similar to our observations in early-induced *Tgfbr2*$^{\Delta eye}$ animals, all of the late-induced *Tgfbr2*$^{\Delta eye}$ mice showed structural changes in the subretinal space that were essentially comparable to that observed in early-induced *Tgfbr2*$^{\Delta eye}$ mice (Fig. 3A, D and 4A, B and C). In focal areas in which photoreceptor outer segments were shortened or completely missing, vessels were observed in the subretinal space. By TEM, a fenestrated endothelial layer was identified surrounding the vessels (Fig. 5B). The RPE in

those areas was multilayered and frequently contained cystic and amorphous inclusions. In six-month-old late-induced *Tgfbr2*$^{\Delta eye}$ mice, the choroid was thickened and photoreceptor outer segments were completely missing (Fig. 4A, B and C). The RPE was reduced to a flat layer or formed focal accumulations in those areas in which subretinal vessels were present. *In vivo* imaging and fluorescein *in vivo* angiography of three-month-old animals showed a regular fundus and retinal vasculature in both control and late-induced *Tgfbr2*$^{\Delta eye}$ mice (Fig. 3C). To investigate the retinal vasculature in more detail, we additionally perfused two-month-old, late-induced *Tgfbr2*$^{\Delta eye}$ mice with high molecular weight FITC-dextran and analyzed the vasculature on meridional sections. The retinal vasculature had a regular appearance and the vessels were in their anatomically correct localization. Furthermore, we did not observe FITC-dextran or fluorescein leaking into the vitreous, the subretinal space or the surrounding tissue (Fig. 3C and E). As we had observed a significant reduction of the pericyte marker neural/glial antigen 2 (NG2) in the retina of early-induced *Tgfbr2*$^{\Delta eye}$ animals[21] we now focused on the coating of the choroidal vessels with NG2 positive pericytes in four-week-old early- and six-week-old late-induced *Tgfbr2*$^{\Delta eye}$ animals. We did not observe a difference in pericyte coverage compared to controls (data not shown). When we analyzed the eyes at the age of six months by *in vivo* fundus imaging and fluorescein angiography, control mice showed again no pathological changes, neither in the fundus, nor in the retinal vasculature (Fig. 4D). In contrast, in late-induced *Tgfbr2*$^{\Delta eye}$ mice the fundus was hyperpigmented indicating RPE proliferation or dedifferentiation, and in some animals the retina had detached (Fig. 4D). In parallel to the structural changes we detected marked functional changes by ERG that reflected the observed gradual degeneration of the retina from three to six months of age in late-induced *Tgfbr2*$^{\Delta eye}$ mice (supplemental Fig. 3A-G). While in three-month-old *Tgfbr2*$^{\Delta eye}$ mice the scotopic responses showed similar waveform but slightly lower amplitudes compared to control mice, the photopic waveform was unchanged in amplitude and implicit time. However, the difference was not statistically significant. In six-month-old *Tgfbr2*$^{\Delta eye}$ mice both, the scotopic and photopic response could not be distinguished from noise in almost all eyes.

Expression of angiogenic factors and immune modulating cytokines in *Tgfbr2*$^{\Delta eye}$ mice

The ‘‘immunovascular axis’’, a crosstalk of the RPE with immune and vascular cells is considered a potent driver of CNV formation.[4] To clarify the mechanisms behind CNV induced by TβRII deletion we consequently analyzed the mRNA expression levels of immune modulating cytokines and markers for the reactivity of Müller glia and microglia cells, respectively. Early-induced *Tgfbr2*$^{\Delta eye}$ mice showed a significant increase in retinal mRNA expression levels of glial fibrillary acidic protein (Gfap), cluster of differentiation (Cd) 68, inducible nitric oxide synthase (iNos), interleukin (Il) -6, tumor necrosis factor (Tnf) -α and monocyte chemoattractant protein-1 (MCP-1/Ccl2) at the age of six weeks compared to control littermates (Fig. 6A). However, in three-month-old late-induced *Tgfbr2*$^{\Delta eye}$ mice, the retinal mRNA expression levels were not significantly enhanced compared to controls; in fact Gfap was even significantly downregulated (Fig. 6B). Next, we used an antibody against F4/80 to label macrophages and microglia cells.[48–50] The number of F4/80 positive cells was significantly ($p \leq 0.05$) increased in the choroid of early-induced *Tgfbr2*$^{\Delta eye}$ animals (142.67 ± 17.13, n = 3) when compared with controls (95.0 ± 8.40, n = 4) (Fig. 6C). The F4/80 positive cells were detected in the subretinal space in close association with the CNV (Fig. 6C). Furthermore, the number of F4/80 positive cells in the retina was significantly increased ($p \leq 0.001$) in early-induced *Tgfbr2*$^{\Delta eye}$ animals (145.75 ± 9.73, n = 4) compared to controls (22.5 ± 1.71, n = 4). Quite similarly three-month-old late-induced *Tgfbr2*$^{\Delta eye}$ animals also presented a distinct accumulation of F4/80 positive cells in the choroid when compared to controls (Fig. 6D). Subsequently, we focused on molecular factors that influence vascular proliferation. In our previously published study, we already showed that early-induced four-week-old *Tgfbr2*$^{\Delta eye}$ mice had significantly elevated mRNA expression levels for the angiogenic factors Vegf-a 120, Vegf-a 164, fibroblast growth factor (Fgf) -2, insulin growth factor (Igf)-1, angiopoetin 2 and platelet derived growth factor (Pdgf)–b compared to control littermates.[21] We now performed immunohistochemistry for VEGF-A to localize the increased levels in the retina of early-induced *Tgfbr2*$^{\Delta eye}$ mice (Fig. 6E). While VEGF-A immunoreactivity was not

detectable in control eyes, there was distinct and intense staining of the ganglion cell layer of early-induced *Tgfbr2*$^{\Delta eye}$ mice. When we screened the retinae of late-induced *Tgfbr2*$^{\Delta eye}$ mice and their control littermates for the expression levels of the Vegf-a isoforms 120 and 164, the expression of Vegf-a 120 was not altered whereas expression of Vegf-a 164 was significantly reduced in five-week-old late-induced *Tgfbr2*$^{\Delta eye}$ mice compared to controls (Fig. 6F). However, at the age of six months, the retinal expression levels of both Vegf-a 120 and 164 were significantly higher in late-induced *Tgfbr2*$^{\Delta eye}$ mice compared to controls. Overall, angiogenic and immune reactivities were much higher in early than in late-induced *Tgfbr2*$^{\Delta eye}$ mice.

Formation of basal lamina deposits in *Tgfbr2*$^{\Delta eye}$ mice

Since CNVs need to find their way across Bruch's membrane (BM) and through the RPE barrier, we used TEM to analyze the structure of both. Control mice showed the regular, five-layered architecture of the BM (Fig. 5A, and B). In early- and late-induced *Tgfbr2*$^{\Delta eye}$ mice though the BM had thickened as result of an accumulation of collagen fibers and fine fibrillar extracellular material was detected between the basal lamina of the choriocapillaris and the elastic layer of BM (Fig. 5A and B). Moreover, in some areas, the RPE basal lamina had been replaced by polymorphous electron dense material that was localized between the elastic layer of BM and the RPE basal infoldings (Fig. 5A). In other areas of the same eye, irregular nodules arising from the RPE basal lamina and with comparable electron density were found between the basal infoldings of the RPE (Fig. 5A). In addition, the basal lamina was frequently found to be interrupted where nodules arised (Fig. 5A and B). Nodules and RPE basal lamina interruptions were found very frequently in early-induced mice and more rarely in late-induced mice. The changes were essentially similar in structure to basal lamina deposits typically found in CNV in humans patients with AMD. Additionally, we found interruptions of the RPE basal lamina with an associated accumulation of electron-dense material in the adjacent RPE infoldings (Fig. 5A). Next, we labeled the basal laminae of RPE and choriocapillaris by collagen type IV immunohistochemistry. In control mice, the basal

laminae of both RPE and choriocapillaris endothelium were continuously labeled (Fig. 5C and D). In early-induced *Tgfbr2*$^{\Delta eye}$ mice continuous staining was only seen in the basal lamina of the choriocapillaris. Staining was irregular and patchy though in region of the RPE (Fig. 5C). In late-induced *Tgfbr2*$^{\Delta eye}$ mice continuous labeling was seen in the basal lamina surrounding choriocapillaris vessels, but was incomplete underneath the RPE (Fig. 5D). In places, the vascular basal lamina reached between RPE cells indicating areas of CNV formation.

Cell-specific conditional deletion of *Tgfbr2* in the RPE and vascular endothelium

Next we aimed at identifying the specific cell type that is responsible for CNV in *Tgfbr2*$^{\Delta eye}$ mice. We focused on the RPE and the vascular endothelium, as endothelial proliferation and breakdown of the RPE barrier are essential requirements for CNV formation. To this end, we generated *Tgfbr2*$^{\Delta RPE}$ mice with *Tgfbr2* deletion specifically in the RPE via doxycycline-driven RPE-specific expression of Cre recombinase. Successful RPE-specific TβRII deletion was confirmed by immunohistochemistry. Control animals showed immunoreactivity for TβRII in photoreceptor outer segments, RPE and choroid. In contrast, immunoreactivity for TβRII in the RPE was not detectable in the RPE of *Tgfbr2*$^{\Delta RPE}$ mice (Supplemental Fig. 2C). In addition, we confirmed recombination by PCR (Supplemental Fig. 2D). We analyzed the ocular morphology of *Tgfbr2*$^{\Delta RPE}$ mice animals in detail by using essentially similar methods as used for *Tgfbr2*$^{\Delta eye}$ mice, but did neither detect choroidal CNV nor other obvious structural changes (Fig. 7 A-D). For generation of *Tgfbr2*$^{\Delta EC}$ mice with specific deletion of TβRII in vascular endothelial cells *VeCad-Cre-ER*^{T2} mice were used with endothelial-specific tamoxifen-inducible Cre expression. Specific recombination in retinal and choroidal vessels was confirmed by GFP immunoreactivity in *VeCad-Cre-ER*^{T2} crossed with *mT/mG* reporter mice (Supplemental Fig. 2E). When analyzing the structure of six-week-old *Tgfbr2*$^{\Delta EC}$ mice the pronounced structural changes that we had reported[21] for early-induced *Tgfbr2*$^{\Delta eye}$ mice such as retinal and vitreal neovascularization, retinal detachment or vitreal hemorrhages were completely absent (Fig. 8A, B). Still, similar to our results seen in early-induced

Tgfbr2$^{\Delta eye}$ mice,[21] dilated vessels were frequently observed in the inner nuclear layer surrounded by electron dense, extravascular material (Fig. 8C and E). Quite intriguingly, at the retinal/choroidal interface, focal areas where frequently observed in which photoreceptor outer segments were degenerated or absent, the RPE multilayered and vascular endothelial cells together with extravasated erythrocytes had accumulated in the subretinal space (Fig. 8D). FITC-dextran perfused ocular sections of *Tgfbr2*$^{\Delta EC}$ mice showed tracer leakage from the choriocapillaris towards the RPE and choroidal vessels penetrating the RPE, indicating a breakdown of the outer blood retinal barrier and the formation of CNV (Fig. 9A). In four-week-old *Tgfbr2*$^{\Delta EC}$ animals and controls, the choroidal vessels were covered by NG2 positive pericytes (data not shown). In contrast to our data from *Tgfbr2*$^{\Delta eye}$ mice though, we did not observe an accumulation of F4/80 positive cells in the choroid of *Tgfbr2*$^{\Delta EC}$ mice (Fig. 9B) (control: 95.0 ± 8.40, n = 4; *Tgfbr2*$^{\Delta EC}$: 111.67 ± 10.41, n = 3; $p \geq 0.05$). In contrast, F4/80 positive cells were increased in the retina (control: 22.5 ± 1.71, n= 4; *Tgfbr2*$^{\Delta EC}$: 108.0 ± 3.51, n = 3, $p \leq 0.001$). In addition, immunoreactivity for collagen IV in the RPE/BM region was seen in basal laminae of choriocapillaris and RPE and did not markedly differ between *Tgfbr2*$^{\Delta EC}$ mice and controls (Fig. 9C). TEM confirmed the findings seen by light microscopy and the presence of degenerated photoreceptor outer segments, multilayered RPE and extravasated erythrocytes (9D). Moreover, plasma-derived electron-dense material did not pass the RPE tight junctions in controls but accumulated between RPE and photoreceptor outer segments *Tgfbr2*$^{\Delta EC}$ mice indicating breakdown of the RPE barrier (Fig. 9E). Overall our data obtained in *Tgfbr2*$^{\Delta EC}$ mice strongly support the conclusion that deletion of TβRII in vascular endothelial cells alone is sufficient to promote the formation of CNV.

Discussion

We conclude that the deletion of TGF-β signaling in the ocular microenvironment is sufficient to induce CNV and other phenotypic characteristics of AMD in humans. Lack of endothelial TGF-β signaling is sufficient to trigger the onset of CNV, while its lack in the RPE is not relevant in this context. This conclusion is based on (1) the generation of mice with TβRII deficiency in the entire microenvironment of the eye, in vascular endothelial cells, or the RPE; (2) the frequent detection of capillaries with fenestrated, PLVAP-positive endothelium that originate from the choriocapillaris and traverse the RPE to anastomose with retinal capillaries; (3) the presence of basal lamina-like deposits around the RPE basal infoldings and of areas with multilayered RPE; and (4) the degeneration of photoreceptor outer segments and (5) the finding of distinct accumulations of F4/80 positive macrophages in the choroid.

TGF-β functions at the retinal/choroidal interface to prevent CNV

The results of our study clearly support the concept that a major function of TGF-β signaling in choroid and retina is the stabilization of the choroidal and retinal vascular beds that are each essential for neuronal integrity in the sensory retina. This function includes the prevention of neoangiogenic processes in the two capillary beds that would otherwise cause neuronal dysfunction and death in the retina. It is of interest though that the sensitivity to the induced lack of TGF-β signaling differs between the two vascular beds, as the formation of microaneurysms, leaky capillaries, and hemorrhages of the retinal vasculature is only seen when TGF-β signaling is deleted in the ocular microenvironment shortly after birth.[21] In contrast, the formation of CNV is seen regardless if TGF-β signaling is interfered with in newborn or three- to four-week-old animals. A likely explanation is the fact that the retinal vasculature of the mouse eye forms and differentiates in the first two weeks after birth[51] and may be more vulnerable to lack of TGF-β signaling during that period. A critical contributing factor may be the failure of pericyte differentiation around retinal capillaries that results from

deficiency of TGF-β signaling during that period.[21] Formation of the choroidal vasculature is completed in late embryonic life and the choriocapillaris is mature at birth.[52]

It is of interest to note, that the coating of the choroidal vessels with NG2 positive pericytes in early- and late-induced *Tgfbr2*$^{\Delta eye}$ *and Tgfbr2*$^{\Delta EC}$ animals was comparable to controls, which appears to indicate that lack of pericyte presence or differentiation is not a requirement for CNV. Data from genetically modified mice with a specific deficiency of PDGF-B in endothelial cells further challenge the role of pericytes in the formation of CNV as these mice show a varying degree of pericyte loss without developing CNV.[53] The higher sensitivity of the choriocapillaris to lack of TGF-β signaling, as opposed to the mature retinal vasculature, may also be caused by the presence of the high amounts of VEGF at the retinal/choroidal interface that are continuously secreted by the RPE, the only source of VEGF in the back of the adult eye.[54] Secretion of VEGF occurs in a polarized fashion to the RPE basolateral side facing the choriocapillaris[55,56] and is expected to convey a proliferative signal to endothelial cells of the choriocapillaris that are no more under the influence of constitutive TGF-β signaling in animals with a deletion of TβRII.

TGF-β and VEGF as part of a homeostatic system to maintain integrity of the choriocapillaris

It is of interest to note that not only VEGF, but also TGF-β1 and -2 are present at high amounts at the retinal/choroidal interface.[20] It is very tempting to speculate that both factors are critical parts of a homeostatic system designed to maintain structure and function of the choriocapillaris. In this system, VEGF would be required to maintain the extreme high density of the choriocapillaris and their fenestrations,[56,57] while TGF-βs antagonize any proliferative properties of VEGF signaling on the vascular endothelium. Failure in the balance of this homeostatic system would cause ablation of the choriocapillaris or induce its proliferation finally leading to CNV (Fig. 10). There is direct evidence for such a homeostatic system from studies in genetically engineered mice in which lack of VEGF and/or increase in TGF-β activity leads to ablation of the choriocapillaris,[14–18] while increase in VEGF[58,59] and/or lack of TGF-β activity (results of our present study) have direct opposite and proliferative effects. For

the initiation of CNV though, lack of TGF-β activity appears to be more relevant than sole increase of VEGF activity, as mice with overexpression of VEGF in the RPE develop an intrachoroidal neovascularization, but no CNV.[58,59] VEGF and TGF-βs induce the transcription of one another in multiple cell types[60–65] and may well do so in the RPE establishing an autoregulatory feedback system designed to maintain structure and function of the choriocapillaris. We realize that this concept needs to be validated in further studies that should also aim at a complete identification of the signaling network that drives endothelial proliferation and CNV formation downstream of TGF-β signaling deficiency.

Potential neuroprotective effects of TGF-β

Late-induced *Tgfbr2*$^{\Delta eye}$ mice showed a dramatic deterioration of the retina. The prolonged presence and formation of CNV, and its detrimental effects on structure and function of the retina may explain this finding. It may also indicate though a participation of TGF-β signaling in a neuroprotective pathway independent of the formation of CNV. We recently showed that TGF-β signaling protects retinal neurons from developmental programmed cell death.[33] It is well possible that it also contributes to maintenance of adult neurons by protecting them from apoptosis. In support of such a scenario are findings reported by Walshe and colleagues who neutralized TGF-β in the adult mouse eye via expression of soluble endoglin, a TGF-β inhibitor.[66] Apoptosis of retinal ganglion cells was observed as were functional deficits detected by ERG. Neuroprotective activities of TGF-βs were reported for multiple types of neurons throughout the central nervous system such as in the striatum,[67] spinal cord,[68] substantia nigra[69] or hippocampus.[70] Quite similarly, there is increasing evidence that also VEGF signaling is important for the trophic maintenance of neurons and their survival after injury, effects that appear to be mediated via the VEGF receptor-2 (VEGFR-2).[71–75] Mice with a constitutive high expression of VEGF in retinal ganglion cells are protected from RGC degeneration after axotomy via VEGFR-2 and downstream activation of ERK1/2 and Akt pathways.[76] While TGF-β/VEGF are antagonists in their actions at the retinal/choroidal

interface and the choriocapillaris, they may cooperate in their neuroprotective activities. Both functions would serve the ultimate goal to maintain structure and function of the retina.

The formation of BlamD-like material is not required for CNV

While CNV was consistently observed in the eyes of both early and late-induced *Tgfbr2*$^{\Delta eye}$ mice, and in that of *Tgfbr2*$^{\Delta EC}$ mice, other findings were predominant only in the eyes of early-induced *Tgfbr2*$^{\Delta eye}$ mice. This includes the formation of homogenous extracellular material between the basal infoldings of the RPE and internal to the RPE basal lamina. The material was quite similar in electron density and structure to that of basal lamina deposits (BlamD), a characteristic finding in patients with early age-related macular degeneration.[77–79] BlamD-like changes were commonly observed in early-induced *Tgfbr2*$^{\Delta eye}$ mice, only rarely in late-induced *Tgfbr2*$^{\Delta eye}$ mice and not in *Tgfbr2*$^{\Delta EC}$ mice suggesting that they are not a requirement for CNV and breakdown of the RPE barrier. Our immunohistochemical data indicate that the homogenous extracellular BlamD-like material contains collagen type IV, an observation that correlates with the observation that basal lamina proteins such as collagen IV and laminin are present in BlamD in human patients with AMD.[77,80] BlamD formation in AMD is likely caused by RPE dysfunction.[78] A comparable dysfunction might more easily happen in early-induced *Tgfbr2*$^{\Delta eye}$ mice, in which the RPE is not yet fully differentiated. Still, a common structural change of the RPE in our models with CNV was the loss of an epithelial monolayer and the formation of multilayered RPE cells. Beneath and above those multilayered RPE cells newly formed vessels were observed, quite similar to type 1 (sub-RPE, occult) and type 2 (sub-retinal, classic) CNV in human patients. Direct deletion of TGF-β signaling in RPE cells appears not to be relevant for formation of BlamD-like material, as it was not observed in *Tgfbr2*$^{\Delta RPE}$ mice.

Neovascularization is associated with macrophage accumulation

A common finding in *Tgfbr2*$^{\Delta eye}$ mice with CNV was the marked accumulation of F4/80 positive macrophages in region of the retinal/choroidal interface. Comparable findings have been described for patients suffering from AMD.[81] It is reasonable to assume that signaling molecules released from proliferative capillary endothelial cells attracted the cells. Reactive macrophages might contribute to the loss of the RPE barrier in our mice and its transition from an epithelial layer to a multilayer in areas of CNV. Our findings in *Tgfbr2*$^{\Delta RPE}$ mice indicate that lack TGF-β signaling in RPE cells is not required for this process. Currently we do not know how proliferating choroidal endothelial cells manage to break through the RPE barrier, but we trust that our mouse models are appropriate tools to identify the causative molecular events. The expression of signaling molecules characteristic for reactive macrophages/microglia such iNos, Il-6, Tnf-α and MCP-1/Ccl was elevated in the retinal mRNA of early-induced *Tgfbr2*$^{\Delta eye}$ mice, but not in late-induced, an observation that we attribute to the marked changes in the inner retina of early-induced mice that are absent in late-induced. Still, those molecules might well be elevated in the microenvironment of the choroidal/retinal interface where macrophages accumulate in mice with CNV.

TGF-β signaling and blood retinal barrier

Leakage of high molecular weight FITC-dextran and erythrocytes into the retina and sub-retinal space, following induced TGF-β signaling deficiency, implicates disruption of the inner and outer blood retinal barriers. Deficiency of the TGF-β signaling pathway in endothelial cells is likely the major contributor in this scenario. Quite comparable, mice with an endothelial specific deficiency of SMAD4, an intracellular downstream mediator of TGF-β signaling, or mice with a deletion of TβRII specifically in endothelial cells in the brain[82,83] show perinatal intracerebral hemorrhages and a breakdown of the blood brain barrier. Furthermore, the virus-driven expression of soluble endoglin results in an inhibition of TGF-β1 signaling in the murine retina, a situation that also causes breakdown of the blood retinal

barrier, most likely mediated through a decreased association of the tight junction proteins occludin and zona occludens (ZO)-1.[66]

TGF-β signaling in human patients with AMD

Several independent case-control genome-wide association studies detected an association of two synonymous polymorphisms in exon 1 of the high-temperature requirement A1 (*HTRA1*) gene with a high risk to develop AMD.[84–86] The gene product HTRA1 appears to play a causative role in CNV.[87–89] Quite intriguingly a recent study provided evidence that the two synonymous HTRA1 variants influence their protein interaction with TGF-β1 leading to an impaired regulation of TGF-β signaling.[90] Moreover, a collaborative genome-wide association study identified *TGFBR1* the gene encoding for the TGF-β1 type I receptor, as a new susceptibility gene for AMD further highlighting the importance of the TGF-β signaling pathway in the context of AMD.[84]

Conclusion

Our findings emphasize the importance of TGF-β signaling as a key player in the development of ocular neovascularization and implicate a fundamental role of TGF-β signaling in the pathogenesis of AMD. A more thorough understanding of this role at the retinal/choroidal interface has the distinct potential to lead to the development of novel treatments strategies preventing CNV in patients suffering from AMD.

Acknowledgements

The authors thank Elke Stauber, Margit Schimmel, Angelika Pach, Silvia Babl and Elfriede Eckert for their excellent technical assistance. This work was funded by DFG Research Unit FOR 1075.

Author contributions

AS, SL, BB performed the majority of the experiments. AS, SL, BB, ET interpreted the data. HJ, AF conducted in-vivo angiography, 3D imaging and ERG experiments. AS, BB, ET wrote the manuscript. BB, ET designed the research studies.

References

1. Friedman DS, O'Colmain BJ, Muñoz B, Tomany SC, McCarty C, de Jong PTVM, Nemesure B, Mitchell P, Kempen J, Eye Diseases Prevalence Research Group: Prevalence of age-related macular degeneration in the United States. Arch Ophthalmol 2004, 122:564–572.

2. Finger RP, Fimmers R, Holz FG, Scholl HPN: Incidence of blindness and severe visual impairment in Germany: projections for 2030. Invest Ophthalmol Vis Sci 2011, 52:4381–4389.

3. Klaver CC, Wolfs RC, Vingerling JR, Hofman A, de Jong PT: Age-specific prevalence and causes of blindness and visual impairment in an older population: the Rotterdam Study. Arch Ophthalmol 1998, 116:653–658.

4. Ambati J, Fowler BJ: Mechanisms of age-related macular degeneration. Neuron 2012, 75:26–39.

5. Lim LS, Mitchell P, Seddon JM, Holz FG, Wong TY: Age-related macular degeneration. Lancet 2012, 379:1728–1738.

6. Fritsche LG, Igl W, Bailey JNC, Grassmann F, Sengupta S, Bragg-Gresham JL, Burdon KP, Hebbring SJ, Wen C, Gorski M, Kim IK, Cho D, Zack D, Souied E, Scholl HPN, Bala E, Lee KE, Hunter DJ, Sardell RJ, Mitchell P, Merriam JE, Cipriani V, Hoffman JD, Schick T, Lechanteur YTE, Guymer RH, Johnson MP, Jiang Y, Stanton CM, Buitendijk GHS, Zhan X, Kwong AM, Boleda A, Brooks M, Gieser L, Ratnapriya R, Branham KE, Foerster JR, Heckenlively JR, Othman MI, Vote BJ, Liang HH, Souzeau E, McAllister IL, Isaacs T, Hall J, Lake S, Mackey DA, Constable IJ, Craig JE, Kitchner TE, Yang Z, Su Z, Luo H, Chen D, Ouyang H, Flagg K, Lin D, Mao G, Ferreyra H, Stark K, von Strachwitz CN, Wolf A, Brandl C, Rudolph G, Olden M, Morrison MA, Morgan DJ, Schu M, Ahn J, Silvestri G, Tsironi EE, Park KH, Farrer LA, Orlin A, Brucker A, Li M, Curcio CA, Mohand-Saïd S, Sahel J-A, Audo I, Benchaboune M, Cree AJ, Rennie CA,

Goverdhan SV, Grunin M, Hagbi-Levi S, Campochiaro P, Katsanis N, Holz FG, Blond F, Blanché H, Deleuze J-F, Igo RP, Truitt B, Peachey NS, Meuer SM, Myers CE, Moore EL, Klein R, Hauser MA, Postel EA, Courtenay MD, Schwartz SG, Kovach JL, Scott WK, Liew G, Tan AG, Gopinath B, Merriam JC, Smith RT, Khan JC, Shahid H, Moore AT, McGrath JA, Laux R, Brantley MA Jr, Agarwal A, Ersoy L, Caramoy A, Langmann T, Saksens NT, de Jong EK, Hoyng CB, Cain MS, Richardson AJ, Martin TM, Blangero J, Weeks DE, Dhillon B, van Duijn CM, Doheny KF, Romm J, Klaver CC, Hayward C, Gorin MB, Klein ML, Baird PN, den Hollander AI, Fauser S, Yates JR, Allikmets R, Wang JJ, Schaumberg DA, Klein BE, Hagstrom SA, Chowers I, Lotery AJ, Léveillard T, Zhang K, Brilliant MH, Hewitt AW, Swaroop A, Chew EY, Pericak-Vance MA, DeAngelis M, Stambolian D, Haines JL, Iyengar SK, Weber BH, Abecasis GR, Heid IM: A large genome-wide association study of age-related macular degeneration highlights contributions of rare and common variants. Nat Genet 2016, 48:134–143.

7. Bhutto I, Lutty G: Understanding age-related macular degeneration (AMD): relationships between the photoreceptor/retinal pigment epithelium/Bruch's membrane/choriocapillaris complex. Mol Aspects Med 2012, 33:295–317.

8. van Lookeren Campagne M, LeCouter J, Yaspan BL, Ye W: Mechanisms of age-related macular degeneration and therapeutic opportunities. J Pathol 2014, 232:151–164.

9. Miller JW, Le Couter J, Strauss EC, Ferrara N: Vascular endothelial growth factor a in intraocular vascular disease. Ophthalmology 2013, 120:106–114.

10. Miller JW: Age-related macular degeneration revisited--piecing the puzzle: the LXIX Edward Jackson memorial lecture. Am J Ophthalmol 2013, 155:1–35.e13.

11. Kur J, Newman EA, Chan-Ling T: Cellular and physiological mechanisms underlying blood flow regulation in the retina and choroid in health and disease. Prog Retin Eye Res 2012, 31:377–406.

12. Bill A, Törnquist P, Alm A: Permeability of the intraocular blood vessels. Trans Ophthalmol Soc U K 1980, 100:332–336.

13. Ford KM, Saint-Geniez M, Walshe T, Zahr A, D'Amore PA: Expression and role of VEGF in the adult retinal pigment epithelium. Invest Ophthalmol Vis Sci 2011, 52:9478–9487.

14. Kurihara T, Westenskow PD, Bravo S, Aguilar E, Friedlander M: Targeted deletion of Vegfa in adult mice induces vision loss. J Clin Invest 2012, 122:4213–4217.

15. Marneros AG, Fan J, Yokoyama Y, Gerber HP, Ferrara N, Crouch RK, Olsen BR: Vascular endothelial growth factor expression in the retinal pigment epithelium is essential for choriocapillaris development and visual function. Am J Pathol 2005, 167:1451–1459.

16. Le Y-Z, Bai Y, Zhu M, Zheng L: Temporal requirement of RPE-derived VEGF in the development of choroidal vasculature. J Neurochem 2010, 112:1584–1592.

17. Saint-Geniez M, Kurihara T, Sekiyama E, Maldonado AE, D'Amore PA: An essential role for RPE-derived soluble VEGF in the maintenance of the choriocapillaris. Proc Natl Acad Sci U S A 2009, 106:18751–18756.

18. Ohlmann A, Scholz M, Koch M, Tamm ER: Epithelial-mesenchymal transition of the retinal pigment epithelium causes choriocapillaris atrophy. Histochem Cell Biol 2016, .

19. Strauss O: The retinal pigment epithelium in visual function. Physiol Rev 2005, 85:845–881.

20. Pfeffer BA, Flanders KC, Guérin CJ, Danielpour D, Anderson DH: Transforming growth factor beta 2 is the predominant isoform in the neural retina, retinal pigment epithelium-choroid and vitreous of the monkey eye. Exp Eye Res 1994, 59:323–333.

21. Braunger BM, Leimbeck SV, Schlecht A, Volz C, Jägle H, Tamm ER: Deletion of ocular transforming growth factor β signaling mimics essential characteristics of diabetic retinopathy. Am J Pathol 2015, 185:1749–1768.

22. Mattapallil MJ, Wawrousek EF, Chan C-C, Zhao H, Roychoudhury J, Ferguson TA, Caspi RR: The Rd8 mutation of the Crb1 gene is present in vendor lines of C57BL/6N mice and embryonic stem cells, and confounds ocular induced mutant phenotypes. Invest Ophthalmol Vis Sci 2012, 53:2921–2927.

23. Chytil A, Magnuson MA, Wright CVE, Moses HL: Conditional inactivation of the TGF-beta type II receptor using Cre:Lox. Genesis 2002, 32:73–75.

24. Hayashi S, McMahon AP: Efficient recombination in diverse tissues by a tamoxifen-inducible form of Cre: a tool for temporally regulated gene activation/inactivation in the mouse. Dev Biol 2002, 244:305–318.

25. Le Y-Z, Zheng W, Rao P-C, Zheng L, Anderson RE, Esumi N, Zack DJ, Zhu M: Inducible expression of cre recombinase in the retinal pigmented epithelium. Invest Ophthalmol Vis Sci 2008, 49:1248–1253.

26. Monvoisin A, Alva JA, Hofmann JJ, Zovein AC, Lane TF, Iruela-Arispe ML: VE-cadherin-CreERT2 transgenic mouse: a model for inducible recombination in the endothelium. Dev Dyn 2006, 235:3413–3422.

27. Boneva SK, Groß TR, Schlecht A, Schmitt SI, Sippl C, Jägle H, Volz C, Neueder A, Tamm ER, Braunger BM: Cre recombinase expression or topical tamoxifen treatment do not affect retinal structure and function, neuronal vulnerability or glial reactivity in the mouse eye. Neuroscience 2016, 325:188–201.

28. Feil R, Brocard J, Mascrez B, LeMeur M, Metzger D, Chambon P: Ligand-activated site-specific recombination in mice. Proc Natl Acad Sci U S A 1996, 93:10887–10890.

766 29. Schlecht A, Leimbeck SV, Tamm ER, Braunger BM: Tamoxifen-Containing Eye Drops
767 Successfully Trigger Cre-Mediated Recombination in the Entire Eye. Adv Exp Med Biol
768 2016, 854:495–500.

769 30. Muzumdar MD, Tasic B, Miyamichi K, Li L, Luo L: A global double-fluorescent Cre
770 reporter mouse. Genesis 2007, 45:593–605.

771 31. Soriano P: Generalized lacZ expression with the ROSA26 Cre reporter strain. Nat
772 Genet 1999, 21:70–71.

773 32. Baulmann DC, Ohlmann A, Flügel-Koch C, Goswami S, Cvekl A, Tamm ER: Pax6
774 heterozygous eyes show defects in chamber angle differentiation that are associated
775 with a wide spectrum of other anterior eye segment abnormalities. Mech Dev 2002,
776 118:3–17.

777 33. Braunger BM, Pielmeier S, Demmer C, Landstorfer V, Kawall D, Abramov N, Leibinger
778 M, Kleiter I, Fischer D, Jägle H, Tamm ER: TGF-β Signaling Protects Retinal Neurons
779 from Programmed Cell Death during the Development of the Mammalian Eye. J
780 Neurosci 2013, 33:14246–14258.

781 34. Karnovsky, M.J.: A formaldehyde-glutaraldehyde fixative of high osmolarity for use in
782 electron microscopy. J Cell Biol 1965, 27:137–138.

783 35. Kugler M, Schlecht A, Fuchshofer R, Kleiter I, Aigner L, Tamm ER, Braunger BM:
784 Heterozygous modulation of TGF-β signaling does not influence Müller glia cell
785 reactivity or proliferation following NMDA-induced damage. Histochem Cell Biol 2015,
786 144:443–455.

787 36. Kugler M, Schlecht A, Fuchshofer R, Schmitt SI, Kleiter I, Aigner L, Tamm ER,
788 Braunger BM: SMAD7 deficiency stimulates Müller progenitor cell proliferation during
789 the development of the mammalian retina. Histochem Cell Biol 2017, .

790 37. Richardson KC, Jarett L, Finke EH: Embedding in epoxy resins for ultrathin sectioning
791 in electron microscopy. Stain Technol 1960, 35:313–323.

792 38. Braunger BM, Ohlmann A, Koch M, Tanimoto N, Volz C, Yang Y, Bösl MR, Cvekl A,
793 Jägle H, Seeliger MW, Tamm ER: Constitutive overexpression of Norrin activates
794 Wnt/β-catenin and endothelin-2 signaling to protect photoreceptors from light damage.
795 Neurobiol Dis 2013, 50:1–12.

796 39. Braunger BM, Ademoglu B, Koschade SE, Fuchshofer R, Gabelt BT, Kiland JA,
797 Hennes-Beann EA, Brunner KG, Kaufman PL, Tamm ER: Identification of adult stem
798 cells in Schwalbe's line region of the primate eye. Invest Ophthalmol Vis Sci 2014,
799 55:7499–7507.

800 40. Wickham H: ggplot2, Elegant Graphics for Data Analysis. New York, NY, Springer New
801 York, 2009, .

802 41. Livak KJ, Schmittgen TD: Analysis of relative gene expression data using real-time
803 quantitative PCR and the 2(-Delta Delta C(T)) Method. Methods 2001, 25:402–408.

804 42. Ertürk A, Becker K, Jährling N, Mauch CP, Hojer CD, Egen JG, Hellal F, Bradke F,
805 Sheng M, Dodt H-U: Three-dimensional imaging of solvent-cleared organs using
806 3DISCO. Nat Protoc 2012, 7:1983–1995.

807 43. Kaufman PL, Adler FH, Levin LA, Alm A: Adler's Physiology of the Eye. Elsevier Health
808 Sciences, 2011, .

809 44. Stan RV, Arden KC, Palade GE: cDNA and protein sequence, genomic organization,
810 and analysis of cis regulatory elements of mouse and human PLVAP genes. Genomics
811 2001, 72:304–313.

812 45. Stan R-V, Kubitza M, Palade GE: PV-1 is a component of the fenestral and stomatal
813 diaphragms in fenestrated endothelia. Proc Natl Acad Sci U S A 1999, 96:13203–
814 13207.

815 46. Stan RV, Tse D, Deharvengt SJ, Smits NC, Xu Y, Luciano MR, McGarry CL, Buitendijk
816 M, Nemani KV, Elgueta R, Kobayashi T, Shipman SL, Moodie KL, Daghlian CP, Ernst
817 PA, Lee H-K, Suriawinata AA, Schned AR, Longnecker DS, Fiering SN, Noelle RJ, Gimi
818 B, Shworak NW, Carrière C: The diaphragms of fenestrated endothelia – gatekeepers
819 of vascular permeability and blood composition. Dev Cell 2012, 23:1203–1218.

820 47. Herrnberger L, Seitz R, Kuespert S, Bösl MR, Fuchshofer R, Tamm ER: Lack of
821 endothelial diaphragms in fenestrae and caveolae of mutant Plvap-deficient mice.
822 Histochem Cell Biol 2012, 138:709–724.

823 48. Hume DA, Perry VH, Gordon S: Immunohistochemical localization of a macrophage-
824 specific antigen in developing mouse retina: phagocytosis of dying neurons and
825 differentiation of microglial cells to form a regular array in the plexiform layers. J Cell
826 Biol 1983, 97:253–257.

827 49. Hume DA, Halpin D, Charlton H, Gordon S: The mononuclear phagocyte system of the
828 mouse defined by immunohistochemical localization of antigen F4/80: macrophages of
829 endocrine organs. Proc Natl Acad Sci U S A 1984, 81:4174–4177.

830 50. Langmann T: Microglia activation in retinal degeneration. J Leukoc Biol 2007, 81:1345–
831 1351.

832 51. Fruttiger M: Development of the mouse retinal vasculature: angiogenesis versus
833 vasculogenesis. Invest Ophthalmol Vis Sci 2002, 43:522–527.

834 52. Rousseau B, Larrieu-Lahargue F, Bikfalvi A, Javerzat S: Involvement of fibroblast
835 growth factors in choroidal angiogenesis and retinal vascularization. Exp Eye Res 2003,
836 77:147–156.

837 53. Enge M, Bjarnegård M, Gerhardt H, Gustafsson E, Kalén M, Asker N, Hammes H-P,
838 Shani M, Fässler R, Betsholtz C: Endothelium-specific platelet-derived growth factor-B
839 ablation mimics diabetic retinopathy. EMBO J 2002, 21:4307–4316.

840 54. Saint-Geniez M, Maldonado AE, D'Amore PA: VEGF expression and receptor activation
841 in the choroid during development and in the adult. Invest Ophthalmol Vis Sci 2006,
842 47:3135–3142.

843 55. Kannan R, Zhang N, Sreekumar PG, Spee CK, Rodriguez A, Barron E, Hinton DR:
844 Stimulation of apical and basolateral VEGF-A and VEGF-C secretion by oxidative stress
845 in polarized retinal pigment epithelial cells. Mol Vis 2006, 12:1649–1659.

846 56. Esser S, Wolburg K, Wolburg H, Breier G, Kurzchalia T, Risau W: Vascular endothelial
847 growth factor induces endothelial fenestrations in vitro. J Cell Biol 1998, 140:947–959.

848 57. Kamba T, Tam BYY, Hashizume H, Haskell A, Sennino B, Mancuso MR, Norberg SM,
849 O'Brien SM, Davis RB, Gowen LC, Anderson KD, Thurston G, Joho S, Springer ML,
850 Kuo CJ, McDonald DM: VEGF-dependent plasticity of fenestrated capillaries in the
851 normal adult microvasculature. Am J Physiol Heart Circ Physiol 2006, 290:H560-576.

852 58. Oshima Y, Oshima S, Nambu H, Kachi S, Hackett SF, Melia M, Kaleko M, Connelly S,
853 Esumi N, Zack DJ, Campochiaro PA: Increased expression of VEGF in retinal
854 pigmented epithelial cells is not sufficient to cause choroidal neovascularization. J Cell
855 Physiol 2004, 201:393–400.

856 59. Schwesinger C, Yee C, Rohan RM, Joussen AM, Fernandez A, Meyer TN, Poulaki V,
857 Ma JJ, Redmond TM, Liu S, Adamis AP, D'Amato RJ: Intrachoroidal neovascularization
858 in transgenic mice overexpressing vascular endothelial growth factor in the retinal
859 pigment epithelium. Am J Pathol 2001, 158:1161–1172.

860 60. Shi X, Guo L-W, Seedial SM, Si Y, Wang B, Takayama T, Suwanabol PA, Ghosh S,
861 DiRenzo D, Liu B, Kent KC: TGF-β/Smad3 inhibit vascular smooth muscle cell

862 apoptosis through an autocrine signaling mechanism involving VEGF-A. Cell Death Dis
863 2014, 5:e1317.

864 61. Jeon S-H, Chae B-C, Kim H-A, Seo G-Y, Seo D-W, Chun G-T, Kim N-S, Yie S-W,
865 Byeon W-H, Eom S-H, Ha K-S, Kim Y-M, Kim P-H: Mechanisms underlying TGF-beta1-
866 induced expression of VEGF and Flk-1 in mouse macrophages and their implications
867 for angiogenesis. J Leukoc Biol 2007, 81:557–566.

868 62. Nam E-H, Park S-R, Kim P-H: TGF-beta1 induces mouse dendritic cells to express
869 VEGF and its receptor (Flt-1) under hypoxic conditions. Exp Mol Med 2010, 42:606–
870 613.

871 63. Park H-YL, Kim JH, Park CK: VEGF induces TGF-β1 expression and myofibroblast
872 transformation after glaucoma surgery. Am J Pathol 2013, 182:2147–2154.

873 64. Li Z-D, Bork JP, Krueger B, Patsenker E, Schulze-Krebs A, Hahn EG, Schuppan D:
874 VEGF induces proliferation, migration, and TGF-beta1 expression in mouse glomerular
875 endothelial cells via mitogen-activated protein kinase and phosphatidylinositol 3-kinase.
876 Biochem Biophys Res Commun 2005, 334:1049–1060.

877 65. Lee KS, Park SJ, Kim SR, Min KH, Lee KY, Choe YH, Hong SH, Lee YR, Kim JS, Hong
878 SJ, Lee YC: Inhibition of VEGF blocks TGF-beta1 production through a PI3K/Akt
879 signalling pathway. Eur Respir J 2008, 31:523–531.

880 66. Walshe TE, Saint-Geniez M, Maharaj ASR, Sekiyama E, Maldonado AE, D'Amore PA:
881 TGF-beta is required for vascular barrier function, endothelial survival and homeostasis
882 of the adult microvasculature. PloS One 2009, 4:e5149.

883 67. Ma M, Ma Y, Yi X, Guo R, Zhu W, Fan X, Xu G, Frey WH, Liu X: Intranasal delivery of
884 transforming growth factor-beta1 in mice after stroke reduces infarct volume and
885 increases neurogenesis in the subventricular zone. BMC Neurosci 2008, 9:117.

886 68. Park SM, Jung JS, Jang MS, Kang KS, Kang SK: Transforming growth factor-beta1
887 regulates the fate of cultured spinal cord-derived neural progenitor cells. Cell Prolif
888 2008, 41:248–264.

889 69. Roussa E, von Bohlen und Halbach O, Krieglstein K: TGF-beta in dopamine neuron
890 development, maintenance and neuroprotection. Adv Exp Med Biol 2009, 651:81–90.

891 70. Zhu Y, Culmsee C, Klumpp S, Krieglstein J: Neuroprotection by transforming growth
892 factor-beta1 involves activation of nuclear factor-kappaB through phosphatidylinositol-3-
893 OH kinase/Akt and mitogen-activated protein kinase-extracellular-signal regulated
894 kinase1,2 signaling pathways. Neuroscience 2004, 123:897–906.

895 71. Carmeliet P, Ruiz de Almodovar C, Carmen R de A: VEGF ligands and receptors:
896 implications in neurodevelopment and neurodegeneration. Cell Mol Life Sci CMLS
897 2013, 70:1763–1778.

898 72. Cvetanovic M, Patel JM, Marti HH, Kini AR, Opal P: Vascular endothelial growth factor
899 ameliorates the ataxic phenotype in a mouse model of spinocerebellar ataxia type 1.
900 Nat Med 2011, 17:1445–1447.

901 73. Ma Y-Y, Li K-Y, Wang J-J, Huang Y-L, Huang Y, Sun F-Y: Vascular endothelial growth
902 factor acutely reduces calcium influx via inhibition of the Ca2+ channels in rat
903 hippocampal neurons. J Neurosci Res 2009, 87:393–402.

904 74. Robinson GS, Ju M, Shih SC, Xu X, McMahon G, Caldwell RB, Smith LE: Nonvascular
905 role for VEGF: VEGFR-1, 2 activity is critical for neural retinal development. FASEB J
906 2001, 15:1215–1217.

907 75. Jin K, Zhu Y, Sun Y, Mao XO, Xie L, Greenberg DA: Vascular endothelial growth factor
908 (VEGF) stimulates neurogenesis in vitro and in vivo. Proc Natl Acad Sci U S A 2002,
909 99:11946–11950.

910 76. Kilic U, Kilic E, Järve A, Guo Z, Spudich A, Bieber K, Barzena U, Bassetti CL, Marti HH,
911 Hermann DM: Human vascular endothelial growth factor protects axotomized retinal
912 ganglion cells in vivo by activating ERK-1/2 and Akt pathways. J Neurosci 2006,
913 26:12439–12446.

914 77. van der Schaft TL, Mooy CM, de Bruijn WC, Bosman FT, de Jong PT:
915 Immunohistochemical light and electron microscopy of basal laminar deposit. Graefes
916 Arch Clin Exp Ophthalmol Albrecht Von Graefes Arch Klin Exp Ophthalmol 1994,
917 232:40–46.

918 78. Curcio CA, Presley JB, Millican CL, Medeiros NE: Basal deposits and drusen in eyes
919 with age-related maculopathy: evidence for solid lipid particles. Exp Eye Res 2005,
920 80:761–775.

921 79. Loeffler KU, Lee WR: Is basal laminar deposit unique for age-related macular
922 degeneration? Arch Ophthalmol 1992, 110:15–16.

923 80. Marshall GE, Konstas AG, Reid GG, Edwards JG, Lee WR: Type IV collagen and
924 laminin in Bruch's membrane and basal linear deposit in the human macula. Br J
925 Ophthalmol 1992, 76:607–614.

926 81. Xu H, Chen M, Forrester JV: Para-inflammation in the aging retina. Prog Retin Eye Res
927 2009, 28:348–368.

928 82. Li F, Lan Y, Wang Y, Wang J, Yang G, Meng F, Han H, Meng A, Wang Y, Yang X:
929 Endothelial Smad4 maintains cerebrovascular integrity by activating N-cadherin through
930 cooperation with Notch. Dev Cell 2011, 20:291–302.

931 83. Nguyen H-L, Lee YJ, Shin J, Lee E, Park SO, McCarty JH, Oh SP: TGF-β signaling in
932 endothelial cells, but not neuroepithelial cells, is essential for cerebral vascular
933 development. Lab Investig J Tech Methods Pathol 2011, 91:1554–1563.

84. Fritsche LG, Chen W, Schu M, Yaspan BL, Yu Y, Thorleifsson G, Zack DJ, Arakawa S, Cipriani V, Ripke S, Igo RP, Buitendijk GHS, Sim X, Weeks DE, Guymer RH, Merriam JE, Francis PJ, Hannum G, Agarwal A, Armbrecht AM, Audo I, Aung T, Barile GR, Benchaboune M, Bird AC, Bishop PN, Branham KE, Brooks M, Brucker AJ, Cade WH, Cain MS, Campochiaro PA, Chan C-C, Cheng C-Y, Chew EY, Chin KA, Chowers I, Clayton DG, Cojocaru R, Conley YP, Cornes BK, Daly MJ, Dhillon B, Edwards AO, Evangelou E, Fagerness J, Ferreyra HA, Friedman JS, Geirsdottir A, George RJ, Gieger C, Gupta N, Hagstrom SA, Harding SP, Haritoglou C, Heckenlively JR, Holz FG, Hughes G, Ioannidis JPA, Ishibashi T, Joseph P, Jun G, Kamatani Y, Katsanis N, N Keilhauer C, Khan JC, Kim IK, Kiyohara Y, Klein BEK, Klein R, Kovach JL, Kozak I, Lee CJ, Lee KE, Lichtner P, Lotery AJ, Meitinger T, Mitchell P, Mohand-Saïd S, Moore AT, Morgan DJ, Morrison MA, Myers CE, Naj AC, Nakamura Y, Okada Y, Orlin A, Ortube MC, Othman MI, Pappas C, Park KH, Pauer GJT, Peachey NS, Poch O, Priya RR, Reynolds R, Richardson AJ, Ripp R, Rudolph G, Ryu E, Sahel JA, Schaumberg DA, Scholl HP, Schwartz SG, Scott WK, Shahid H, Sigurdsson H, Silvestri G, Sivakumaran TA, Smith RT, Sobrin L, Souied EH, Stambolian DE, Stefansson H, Sturgill-Short GM, Takahashi A, Tosakulwong N, Truitt BJ, Tsironi EE, Uitterlinden AG, van Duijn CM, Vijaya L, Vingerling JR, Vithana EN, Webster AR, Wichmann HE, Winkler TW, Wong TY, Wright AF, Zelenika D, Zhang M, Zhao L, Zhang K, Klein ML, Hageman GS, Lathrop GM, Stefansson K, Allikmets R, Baird PN, Gorin MB, Wang JJ, Klaver CC, Seddon JM, Pericak-Vance MA, Iyengar SK, Yates JR, Swaroop A, Weber BH, Kubo M, Deangelis MM, Léveillard T, Thorsteinsdottir U, Haines JL, Farrer LA, Heid IM, Abecasis GR; AMD Gene Consortium: Seven new loci associated with age-related macular degeneration. Nat Genet 2013, 45:433–439, 439e1-2.

85. Yang Z, Camp NJ, Sun H, Tong Z, Gibbs D, Cameron DJ, Chen H, Zhao Y, Pearson E, Li X, Chien J, Dewan A, Harmon J, Bernstein PS, Shridhar V, Zabriskie NA, Hoh J, Howes K, Zhang K: A variant of the HTRA1 gene increases susceptibility to age-related macular degeneration. Science 2006, 314:992–993.

962 86. Dewan A, Liu M, Hartman S, Zhang SS-M, Liu DTL, Zhao C, Tam POS, Chan WM, Lam
963 DSC, Snyder M, Barnstable C, Pang CP, Hoh J: HTRA1 promoter polymorphism in wet
964 age-related macular degeneration. Science 2006, 314:989–992.

965 87. Vierkotten S, Muether PS, Fauser S: Overexpression of HTRA1 leads to ultrastructural
966 changes in the elastic layer of Bruch's membrane via cleavage of extracellular matrix
967 components. PloS One 2011, 6:e22959.

968 88. Zhang L, Lim SL, Du H, Zhang M, Kozak I, Hannum G, Wang X, Ouyang H, Hughes G,
969 Zhao L, Zhu X, Lee C, Su Z, Zhou X, Shaw R, Geum D, Wei X, Zhu J, Ideker T, Oka C,
970 Wang N, Yang Z, Shaw PX, Zhang K: High Temperature Requirement Factor A1
971 (HTRA1) Gene Regulates Angiogenesis through Transforming Growth Factor-β Family
972 Member Growth Differentiation Factor 6. J Biol Chem 2012, 287:1520–1526.

973 89. Nakayama M, Iejima D, Akahori M, Kamei J, Goto A, Iwata T: Overexpression of HtrA1
974 and exposure to mainstream cigarette smoke leads to choroidal neovascularization and
975 subretinal deposits in aged mice. Invest Ophthalmol Vis Sci 2014, 55:6514–6523.

976 90. Friedrich U, Datta S, Schubert T, Plössl K, Schneider M, Grassmann F, Fuchshofer R,
977 Tiefenbach K-J, Längst G, Weber BHF: Synonymous variants in HTRA1 implicated in
978 AMD susceptibility impair its capacity to regulate TGF-β signaling. Hum Mol Genet
979 2015, 24:6361–6373.

980

Tables

Table 1. Treatment time points and performed analyses

Mouse model	Treatment	Performed analyses	Age
Tgfbr2$^{\Delta eye}$ and controls	Tamoxifen P4-P8	Morphology	2 and 3 months
		FITC-Dextran	6 weeks
		3D-Imaging	6 weeks
		Electron microscopy	2.5 months
		RNA Analyses	6 weeks
		Immunohistochemistry	4 and 6 weeks
Tgfbr2$^{\Delta eye}$ and controls	Tamoxifen P21-P25	Morphology	3 and 6 months
		FITC-Dextran	2 months
		Angiography	3 and 6 months
		ERG	3 and 6 months
		Electron microscopy	3 months
		RNA Analyses	5 weeks
		Immunohistochemistry	3 months
Tgfbr2$^{\Delta EC}$ and controls	Tamoxifen P4-P8	Morphology	6 weeks
		FITC-Dextran	6 weeks
		Electron microscopy	4 and 6 weeks
		Immunohistochemistry	4 and 6 weeks
Tgfbr2$^{\Delta RPE}$ and controls	Doxycyclin P21-P25	Morphology	6 months
		Angiography	6 months

985 **Table 2.** Antibodies used for immunohistochemistry

Primary antibody	Fixation	Secondary antibody
TβRII- L21 (Santa Cruz) 1:20	4% paraformaldehyde (PFA)	anti-rabbit, biotinylated (Vector) 1:500, Streptavidin Alexa 488 (Invitrogen) 1:1000
Collagen IV (Rockland) 1:100	4% PFA	anti-rabbit Cy™-3 conjugated (Jackson Immuno Research Lab) 1:2000
VEGF-a 1:50 (R&D systems)	4% PFA	anti-goat, biotinylated (Vector) 1:500, Streptavidin Alexa 546 (Invitrogen) 1:1000
F4/80 (Acris Antibodies) 1:600	4% PFA	anti-rat Cy™-3 conjugated (Jackson Immuno Research Lab) 1:2000 in PBS
PLVAP (Santa Cruz) 1:50	4%PFA	anti-rat Cy™-3 conjugated (Jackson Immuno Research Lab) 1:2000

986

987

988 **Table 3.** Primers used for real time PCR amplification

Gene	Sequence forward	Sequence reverse
GAPDH	5'-TGTCCGTCGTGGATCTGAC-3'	5'-CCTGCTTCACCACCTTCTTG-3'
GNB2L	5'-TCTGCAAGTACACGGTCCAG-3'	5'-ACGATGATAGGGTTGCTGCT-3'
RPL32	5'-GCTGCCATCTGTTTTACGG-3'	5'-TGACTGGTGCCTGATGAACT-3'
Tgfbr2	5'-AGAAGCCGCATGAAGTCTG-3'	5'-GGCAAACCGTCTCCAGAGTA-3'
Ccl2	5'-CATCCACGTGTTGGCTCA-3'	5'-GATCATCTTGCTGGTGAATGAGT-3'
Cd68	5'-CTCTCTAAGGCTACAGGCTGCT-3'	5'-TCACGGTTGCAAGAGAAACA-3'
Gfap	5`-TCGAGATCGCCACCTACAG.3´	5`-GTCTGTACAGGAATGGTGATGC-3`
Il6	5'-GCTACCAAACTGGATATAATCAGGA-3'	5'-CCAGGTAGCTATGGTACTCCAGAA-3'
iNos	5'-GGGCTGTCACGGAGATCA-3'	5'-CCATGATGGTCACATTCTGC-3'
Tnf-α	5'-TCTTCTCATTCCTGCTTGTGG-3'	5'-GGTCTGGGCCATAGAACTGA-3'
Vegf-a-120	5'-AAAGCCAGCACATAGGAGAG-3'	5'-GGCTTGTCACATTTTTCTGG-3'
Vegf-a-164	5'-GAACAAAGCCAGAAAATCACTGTG-3'	5'-CGAGTCTGTGTTTTTGCAGGAAC-3'
Fgf2	5'-CGGCTCTACTGCAAGAACG-3'	5'-TGCTTGGAGTTGTAGTTTGACG-3'

989

Figures legends

Figure 1. Early-induced deletion of TGF-β signaling in the eye causes structural changes in the subretinal space.

Richardson stained semithin sections (1 µm thick) of an early-induced *Tgfbr2*$^{\Delta eye}$ mouse and its control littermate. (**A**) Retinal hemispheres of two-month-old control and *Tgfbr2*$^{\Delta eye}$ animals. Scale bars = 200µm. (**B)** Detailed magnification of the retina. The control mouse shows regular structure. In the retina of the *Tgfbr2*$^{\Delta eye}$ mouse a vessel (asterisk) filled with erythrocytes is seen, which disrupts the inner (INL) and outer nuclear layer (ONL) and is surrounded by an accumulation of cells that continue into the subretinal space (arrows). In the subretinal space mononuclear cells (arrowhead) are present while photoreceptor outer segments are degenerated and the choroid is thickened. Scale bars = 20µm. (**C)** Left-handed panel. In the inner retina of two-month-old *Tgfbr2*$^{\Delta eye}$ mice accumulations of endothelial cells are seen in both the outer nuclear/plexiform layer (ONL/OPL) and in the inner nuclear/plexiform layer (INL/IPL). Right-handed panel. At the retinal/choroidal interface of two- and three-month-old Tgfbr2$^{\Delta eye}$ mice the RPE is multilayered (black arrows in upper panel) and contains cystic and amorphous inclusions (upper panel, black arrowhead). At the age of three months erythrocyte-containing vessels fill the subretinal space (middle and lower panel, black arrowheads). Scale bars = 20µm. IPL, inner plexiform layer; OS, outer segments; IS, inner segments; INL, inner nuclear layer; RPE, retinal pigment epithelium.

Figure 2. Subretinal neovascularization with fenestrated endothelium following deletion of TGF-β signaling in the eyes of early-induced *Tgfbr2*$^{\Delta eye}$ mice.

(A) FITC-dextran (green)-perfused retinal meridional section of a control and *Tgfbr2*$^{\Delta eye}$ mouse at 6 weeks of age. White arrows point towards choroidal vessels breaking through Bruch's membrane and RPE (nuclei of the RPE marked by white arrowheads) into the subretinal space. Nuclei are DAPI-stained (blue). Scale bars = 50µm. (**B)** Light-sheet fluorescence microscopy of transparent eyes of six-week-old lectin-injected *Tgfbr2*$^{\Delta eye}$ mice and a control littermate. The control mouse shows an essentially regular arborized retinal

vasculature. The *Tgfbr2*$^{\Delta eye}$ mice have an irregular arrangement of the retinal plexus and form anastomoses between retinal and choroidal vessels (arrows). (**C)** Transmission electron microscopy of an intraretinal vessel outlined with a continuous endothelium (cE) in a 2.5-month-old control animal. In contrast, the subretinal neovasculature in the *Tgfbr2*$^{\Delta eye}$ littermate has a fenestrated endothelium (fE, black arrows). Scale bars = 1000nm (left and right panel), 5000 nm (middle panel). (**D)** Immunoreactivity for PLVAP (red) in the retina at 4 weeks of age. The control and the *Tgfbr2*$^{\Delta eye}$ animal show a thin, one-layered PLVAP signal in the choriocapillaris (white arrowheads). In addition, the *Tgfbr2*$^{\Delta eye}$ mouse displays PLVAP-positive signals (white arrows) in RPE and subretinal space. Nuclei are DAPI-stained (blue). Scale bars = 50µm. RGC, retinal ganglion cells; INL, inner nuclear layer; ONL, outer nuclear layer; RPE, retinal pigment epithelium; C, choroid; BM, Bruch's membrane; RPE retinal pigment epithelium; fE, fenestrated endothelium; cE, continuous endothelium; E, endothelium; CC, choriocapillaris.

Figure 3. Subretinal neovascularization following deletion of TGF-β signaling in the eyes of three-month-old late-induced *Tgfbr2*$^{\Delta eye}$ mice.

(A) Richardson's stained semithin sections (1µm thick) of the retinal hemispheres of a three-month-old, late-induced *Tgfbr2*$^{\Delta eye}$ mouse and its control littermate. Scale bars = 500µm. (**B)** Higher magnification of the retinal sections. Scale bars = 50µm. (**C)** *In vivo* funduscopy and fluorescein angiography of a three-month-old, late-induced *Tgfbr2*$^{\Delta eye}$ mouse and its control littermate. The retinal vasculature and the fundus appear essentially normal. (**D)** Detailed magnification of Richardson stained semithin sections of the retinal/choroidal interface of three-month-old *Tgfbr2*$^{\Delta eye}$ mice and a control littermate. The control mouse shows regular structure. *Tgfbr2*$^{\Delta eye}$ mice show focal areas in which the photoreceptor outer segments are shortened or completely missing with vessels in the subretinal space. In these regions, the RPE is multilayered (white arrowheads, lower panel) and frequently contains cystic and amorphous inclusions (white arrow, middle panel). Mononuclear cells (white arrowhead, middle panel) are visible in the subretinal space. Scale bars = 20µm. (**E)** FITC-dextran (green) perfused retinal meridional section of a two-month-old *Tgfbr2*$^{\Delta eye}$ mouse. The three

retinal vascular plexus are present in their correct localization. Nuclei are DAPI-stained (blue). Scale bars = 50µm. INL, inner nuclear layer; ONL, outer nuclear layer; RPE, retinal pigment epithelium; C, choroid.

Figure 4. Subretinal neovascularization and retinal degeneration following deletion of TGF-β signaling in the eyes of six-month-old late-induced *Tgfbr2*$^{\Delta eye}$ mice

(A) Richardson's stained semithin sections (1µm) of the retinal hemispheres of six-month-old animals. The control animal shows regular retinal morphology. In contrast, in the *Tgfbr2*$^{\Delta eye}$ littermate photoreceptor outer segments are completely degenerated. Scale bars = 500µm. (**B)** Detailed magnification of Richardson's stained semithin sections of the outer retina and the choroid of six-month-old *Tgfbr2*$^{\Delta eye}$ mice and a control littermate. The morphology of the control mouse is normal. In contrast, the *Tgfbr2*$^{\Delta eye}$ mouse has erythrocyte-filled vessels in the RPE (upper *Tgfbr2*$^{\Delta eye}$ panel, arrowheads), areas with a thickened (middle *Tgfbr2*$^{\Delta eye}$ panel) and thinned (lower *Tgfbr2*$^{\Delta eye}$ panel) RPE and an accumulation of pigmented cells in the sensory retina (upper, middle and lower *Tgfbr2*$^{\Delta eye}$ panel, arrows). Scale bars = 20µm. (**C)** Detailed magnification of the retina. In the *Tgfbr2*$^{\Delta eye}$ mouse the retina is degenerated with a complete loss of photoreceptors. The RPE is disorganized, pigmented cells accumulate in the sensory retina and the choroid is thickened. Scale bars = 50µm. (**D)** *In vivo* funduscopy and fluorescein angiography of the control animal are normal. *Tgfbr2*$^{\Delta eye}$ mice show a hyperpigmented fundus (middle panel) or retinal detachment (right-handed panel). RGC, retinal ganglion cells; INL, inner nuclear layer; IPL, inner plexiform layer; PS, photoreceptor segments; RPE, retinal pigment epithelium. C, choroid.

Figure 5. Structural changes of Bruch's membrane (BM) in early and late-induced *Tgfbr2*$^{\Delta eye}$ mice. **(A)** Transmission electron microscopy (TEM) of RPE/BM in early-induced 2.5-month-old mice. Upper panel: The BM of the control is of regular structure, but thickened in Tgfbr2$^{\Delta eye}$ mice as result of an accumulation of collagen fibers and fine fibrillar extracellular material between the basal lamina of the choriocapillaris and the elastic layer of BM. In some areas (right-handed panel) the RPE basal lamina is replaced by polymorphous electron dense material that reaches from the elastic layer of BM to the RPE basal infoldings. Lower panel: In other RPE/BM areas of early-induced *Tgfbr2*$^{\Delta eye}$ mice irregular nodules arise from the RPE basal lamina (arrows) and extend between the basal infoldings of the RPE. In places (arrowhead, right-handed panel) the RPE basal lamina is interrupted where nodules arise. Scale bars = 500nm. (**B**) TEM of RPE/BM in three-month-old late-induced Tgfbr2$^{\Delta eye}$ mice. RPE/BM are of regular structure in control mice, but thickened in Tgfbr2$^{\Delta eye}$ mice. Erythrocyte (Er)-filled vessels with fenestrated endothelium (arrow) are seen between RPE and photoreceptor outer segments (upper row, right-hand panel, inset). In places, the RPE basal lamina is interrupted (arrow) and electron dense nodules arise to extend between the basolateral RPE infoldings (Lower row, middle panel. Higher magnification, right-handed panel). Scale bars = 500nm (upper panel), 250nm (lower panel). (**C)** Immunoreactivity for collagen IV (red) of the retinal/choroidal interface in early-induced, four-week-old Tgfbr2$^{\Delta eye}$ mice. In the control, the basal laminae of RPE and choriocapillaris endothelium are labeled. In Tgfbr2$^{\Delta eye}$ mice staining is seen in the basal lamina of the choriocapillaris. Staining is irregular and patchy in region of the RPE. Nuclei are DAPI-stained (blue). RPE nuclei are marked by arrowheads. Scale bars = 50µm. (**D)** Immunoreactivity for collagen IV (red) in the retinal/choroidal interface in late-induced, three-month-old Tgfbr2$^{\Delta eye}$ mice. In the control, the basal laminae of RPE and choriocapillaris endothelium are continuously labeled. In Tgfbr2$^{\Delta eye}$ mice labeling is seen in the basal lamina surrounding choriocapillaris vessels, but is incomplete underneath the RPE. In places, the vascular basal lamina continues between RPE cells (arrows) indicating areas of CNV. Nuclei are DAPI-stained (blue). Scale bars =

50µm. RPE nuclei are marked by arrowheads. RPE, retinal pigment epithelium; BM, Bruch's membrane; CC, choriocapillaris, ONL, outer nuclear layer; Er. erythrocyte.

Figure 6. Expression of angiogenic and immune-modulating molecules in early- and late-induced *Tgfbr2*$^{\Delta eye}$ mice

(A/B) Real-time RT-PCR for mRNA of Gfap, CD68, iNOS, Ccl2, IL6, Tnf-α in six-week-old early-induced *Tgfbr2*$^{\Delta eye}$ mice and controls (**A**) and five-week old late-induced *Tgfbr2*$^{\Delta eye}$ mice (**B**) and controls. (**C)** FITC-dextran (green) perfused and F4/80 (red) immunostained sections of a six-week-old early-induced *Tgfbr2*$^{\Delta eye}$ mouse and control. The control mouse shows weak immunoreactivity for F4/80 (red) positive cells in the choroid. In *Tgfbr2*$^{\Delta eye}$ mice, the choroidal immunoreactivity for F4/80 (red) is more pronounced and numerous F4/80 positive cells accumulate in the subretinal space and in close association to choroidal vessels penetrating the RPE (arrowhead). Nuclei are DAPI-stained (blue). Scale bars = 50µm. (**D)** F4/80 (red) immunostained sections of a three-month-old, late-induced *Tgfbr2*$^{\Delta eye}$ mouse and control. A weak signal for F4/80 is visible in the choroid of the control mouse. In contrast, the *Tgfbr2*$^{\Delta eye}$ mouse shows numerous F4/80 positive cells in the choroid. Nuclei are DAPI-stained (blue). Scale bars = 20µm. (**E)** Immunoreactivity for VEGF-A (red) in early-induced four-week-old mice. The control mouse has a faint immunoreactivity for VEGF-A, which is increased in the Tgfbr2$^{\Delta eye}$ mouse. Nuclei are DAPI-stained (blue). Scale bars = 50µm. (**F)** Real-time RT-PCR for mRNA of Vegf-a 120, Vegf-a 164 in late-induced five-week (left panel) and six-month-old mice (right panel). Data are expressed as mean ± SEM. Early-induced mice: Control, n ≥ 7, *Tgfbr2*$^{\Delta eye}$: n ≥ 7, Student's *t*-test. Late-induced mice (5 weeks old), Control, n ≥ 6, *Tgfbr2*$^{\Delta eye}$, n ≥ 2, Student's *t*-test. Late-induced mice (six months old), Control, n= 9, *Tgfbr2*$^{\Delta eye}$, n = 7, Student's *t*-test. *$P \leq 0.05$, **$P \leq 0.01$.

Figure 7. Deletion of TGFβ-signaling in the RPE

Richardson's stained semithin sections. (**A)** Retinal hemispheres of six-month-old animals. The control mouse and the *Tgfbr2*$^{\Delta RPE}$ mouse do not obviously differ in structure. Scale bars = 500µm. (**B)** Detailed magnification of retina/choroid in a *Tgfbr2*$^{\Delta RPE}$ mouse and its control littermate showing an essentially normal morphology. Scale bars = 50µm. (**C)** *In vivo* funduscopy and fluorescein angiography show no obvious alterations in the *Tgfbr2*$^{\Delta RPE}$ mouse compared to the control. (**D)** Detailed magnifications of the interface of the outer retina, RPE and choroid, again showing a regular morphology in the*Tgfbr2*$^{\Delta RPE}$ mice and controls. Scale bars = 20µm. RGC, retinal ganglion cells; INL, inner nuclear layer; ONL, outer nuclear layer; RPE, retinal pigment epithelium.

Figure 8. Structural changes of the retina in *Tgfbr2*$^{\Delta EC}$ mice

Richardson stained semithin sections of a six-week-old *Tgfbr2*$^{\Delta EC}$ mouse and its control littermate. (**A)** Retinal hemispheres of the control mouse and the Tgfbr2$^{\Delta EC}$ littermate. Scale bars = 200µm. (**B)** Detailed magnification of the retina and choroid. Scale bars = 50µm. (**C)** Dilated retinal vessels (white arrowheads) are seen in the INL of *Tgfbr2*$^{\Delta EC}$ mice. Scale bars = 20µm. (**D)** In the retinal/choroidal interface, endothelial cells (white arrows), erythrocytes (white arrowheads), mononuclear cells (black arrowhead) and ragged edged extravascular material (black arrow) are seen between degenerating photoreceptor outer segments. Scale bars = 20µm. **(E)** Transmission electron microscopy (TEM) of an intraretinal vessel in a six-week-old *Tgfbr2*$^{\Delta EC}$ animal. Electron-dense material is visible around the intraretinal vessel (left panel). The boxed region is shown in higher magnification (right panel). The arrowheads point to the electron-dense extravascular material with ragged edged appearance. Scale bars = 1000nm. RGC, retinal ganglion cells; IPL, inner plexiform layer; INL, inner nuclear layer; ONL, outer nuclear layer; RPE, retinal pigment epithelium; Er, erythrocyte.

Figure 9. Structural changes of the retinal/choroidal interface in *Tgfbr2*$^{\Delta EC}$ mice

(A) FITC-dextran perfused retinal meridional sections of a six-week-old *Tgfbr2*$^{\Delta EC}$ mouse and its control littermate. White arrows point towards tracer leakage in the RPE (middle panel) and choroidal vessels (right panel) invading the RPE. Nuclei are DAPI-stained (blue). Scale bars = 50µm. (**B)** FITC-dextran (green) perfused and F4/80 (red) immunostained sections. The control and the *Tgfbr2*$^{\Delta EC}$ littermate show immunoreactivity for F4/80 (red) positive cells in the choroid, which are not higher in number in the mutant. Nuclei are DAPI-stained (blue). Scale bars = 20µm. (**C)** Immunoreactivity for collagen IV (red) in the RPE/BM region of six-week-old mice. Basal laminae of choriocapillaris and RPE are regularly labeled in control and mutant. Nuclei are DAPI-stained (blue), RPE nuclei are marked by arrowheads. (**D, E)** TEM of RPE/BM in four to six-week-old mice. Scale bars = 20µm. (**D**) In the control, photoreceptor outer segments, RPE and BM are of normal structure. In the *Tgfbr2*$^{\Delta EC}$ mouse, areas of degenerated photoreceptor outer segments, multilayered RPE (black arrowheads point towards nuclei of RPE cells) and extravasated erythrocytes are present Scale bars = 1000nm. (**E)**. Plasma-derived electron-dense material does not pass the RPE tight junctions in controls (arrowheads). In contrast, in the mutant it accumulates between RPE and photoreceptor outer segments (arrowheads). Scale bars = 500nm. Er, erythrocyte; RPE, retinal pigment epithelium; BM, Bruch`s membrane; ONL, outer nuclear layer.

Figure 10. Schematic of signaling events at the retinal–choroidal interface

Normally the RPE secretes high amounts of both TGF-β and VEGF that both ensure an appropriate physiological microenvironment for the choriocapillaris including its VEGF-mediated maintenance and TGF-β-mediated inhibition of proliferation (right). The deletion of *Tgfbr2* in endothelial cells results in the specific disability of TGF-β to act on endothelial cells (red cross). This results in an imbalance of the effects of VEGF/TGF-β, a scenario that promotes the proliferation of the vascular endothelium of the choriocapillaris in direction of the RPE and finally results in CNV. TGF-β, transforming growth factor-β; VEGF, vascular

endothelial growth factor; RPE, retinal pigment epithelium; CNV, choroidal neovascularization.

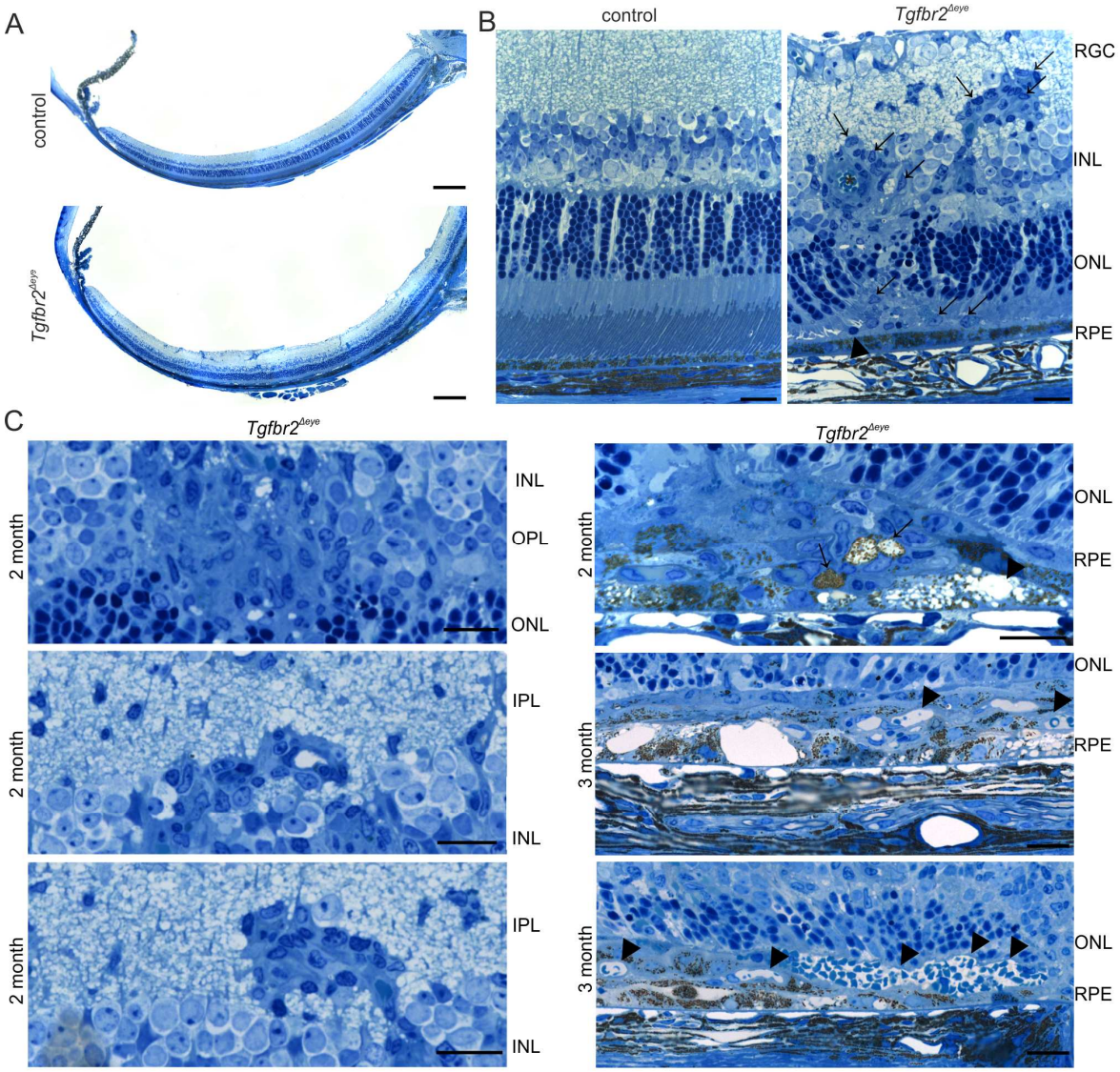
A
control
Tgfbr2Δeye
B
control
Tgfbr2Δeye
RGC
INL
ONL
RPE
C
Tgfbr2Δeye
2 month
INL
OPL
ONL
2 month
IPL
INL
2 month
IPL
INL
Tgfbr2Δeye
2 month
ONL
RPE
3 month
ONL
RPE
3 month
ONL
RPE

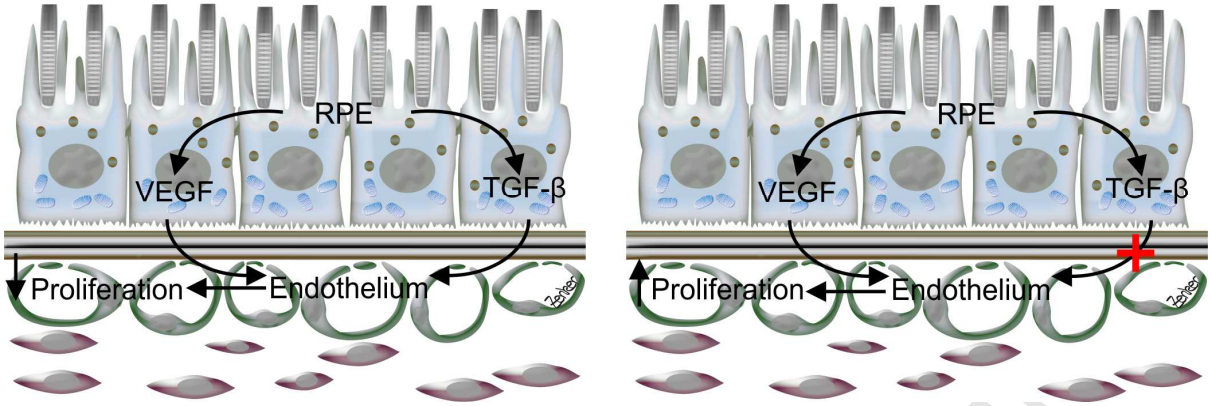

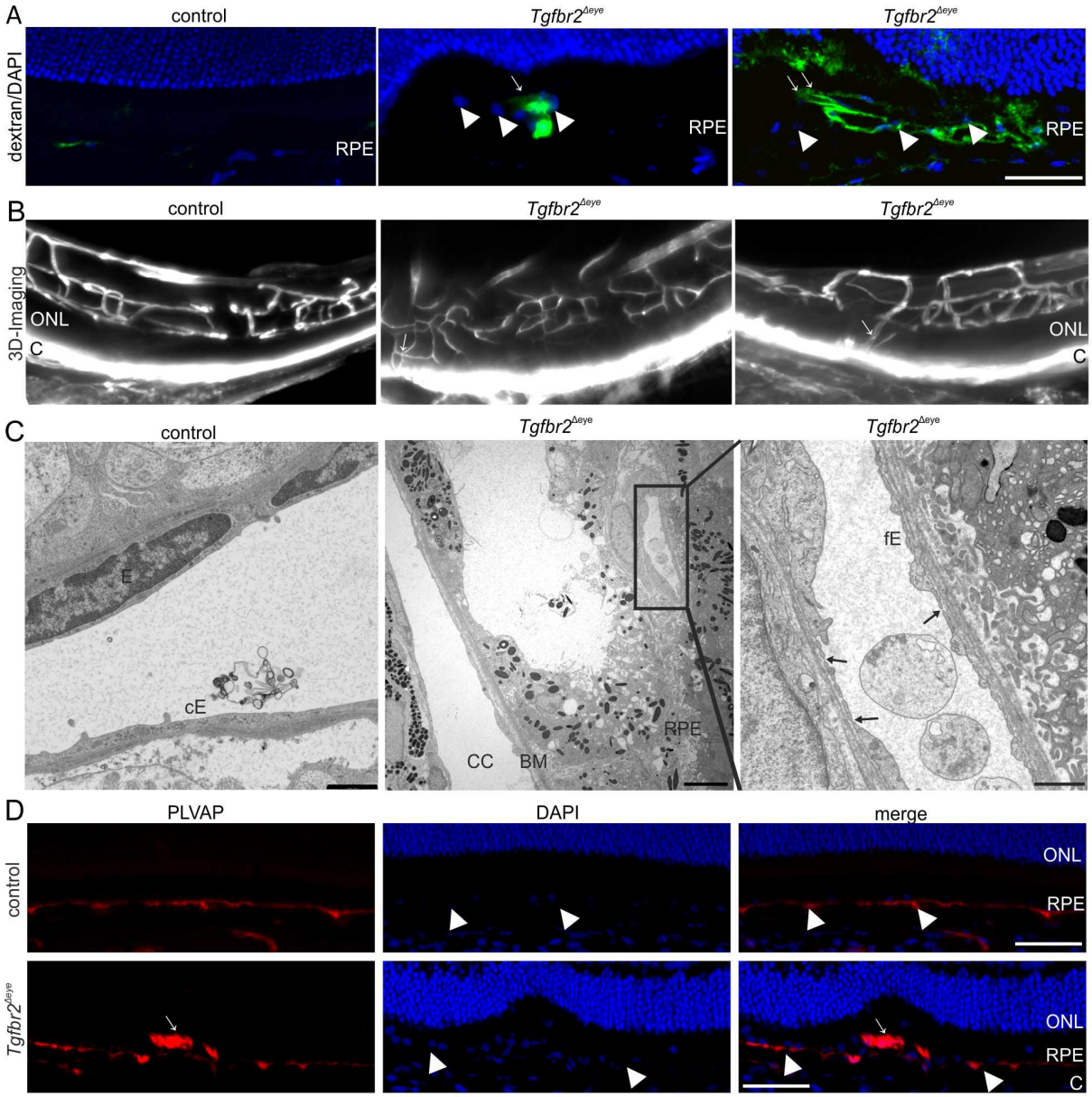
A
control
Tgfbr2Δeye
Tgfbr2Δeye
dextran/DAPI
RPE
RPE
RPE
B
control
Tgfbr2Δeye
Tgfbr2Δeye
3D-Imaging
ONL
C
ONL
C
C
control
Tgfbr2Δeye
Tgfbr2Δeye
E
cE
CC
BM
RPE
fE
D
PLVAP
DAPI
merge
control
Tgfbr2Δeye
ONL
RPE
ONL
RPE
C

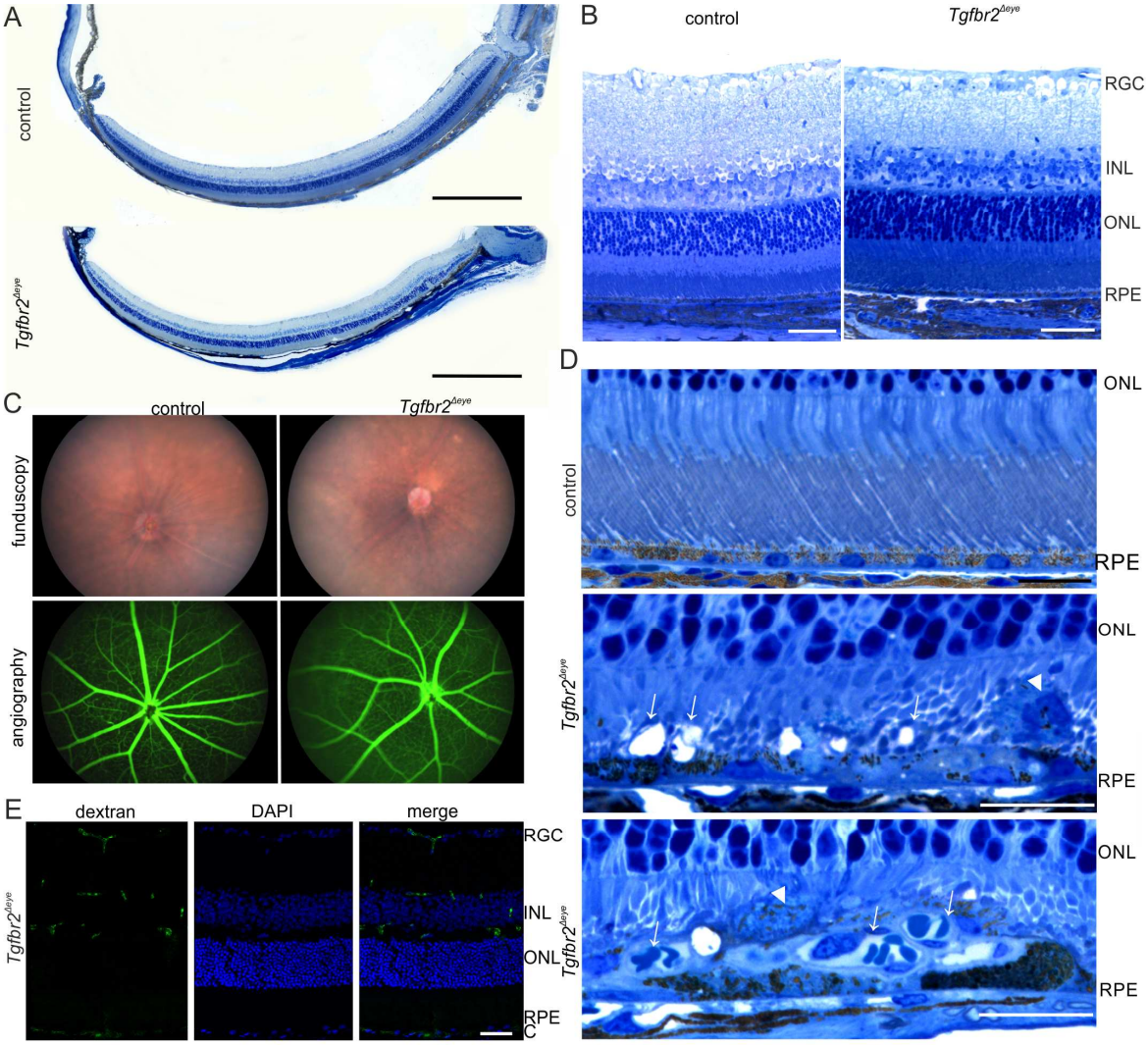

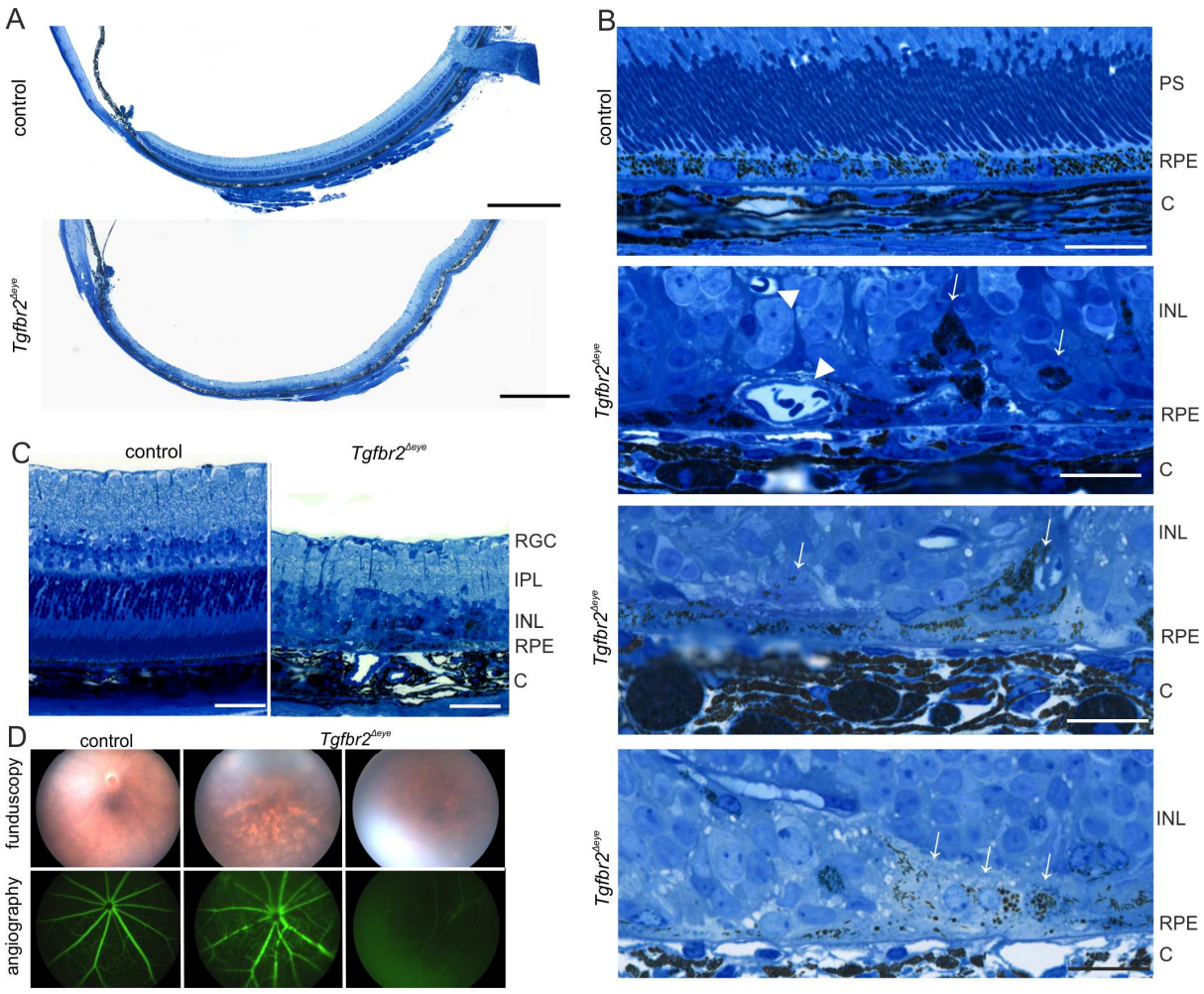
A
control
Tgfbr2Δeye
B
control
PS
RPE
C
Tgfbr2Δeye
INL
RPE
C
Tgfbr2Δeye
INL
RPE
C
Tgfbr2Δeye
INL
RPE
C
C
control
Tgfbr2Δeye
RGC
IPL
INL
RPE
C
D
control
Tgfbr2Δeye
funduscopy
angiography

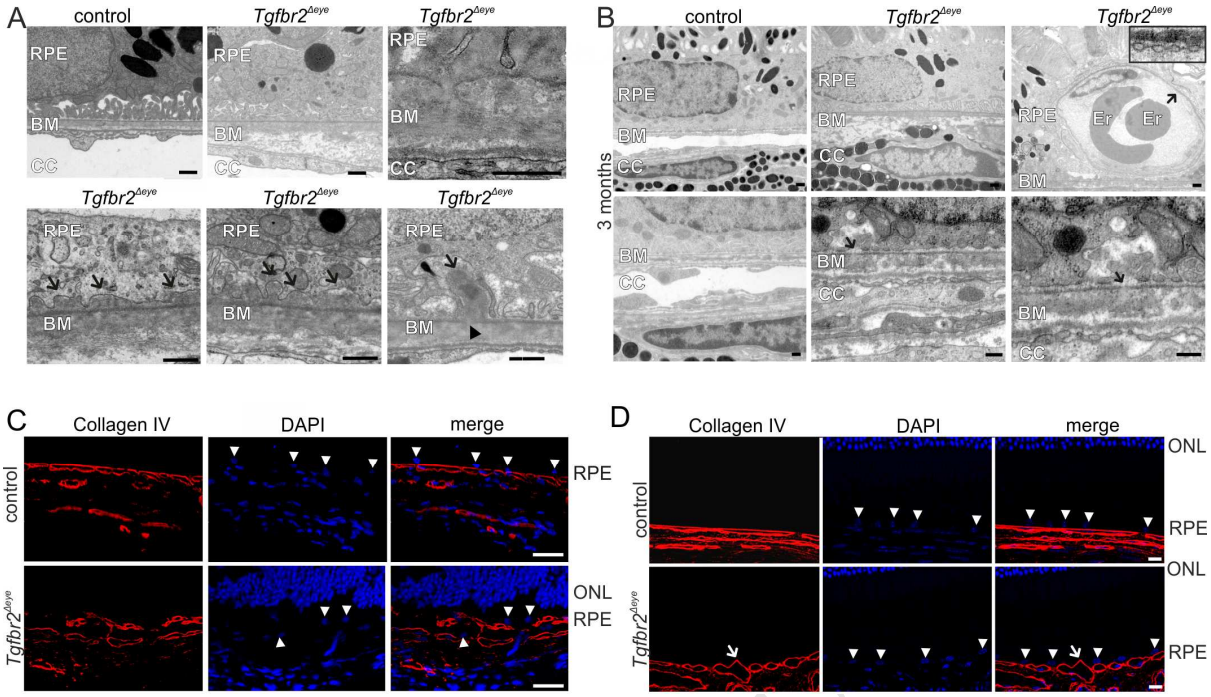

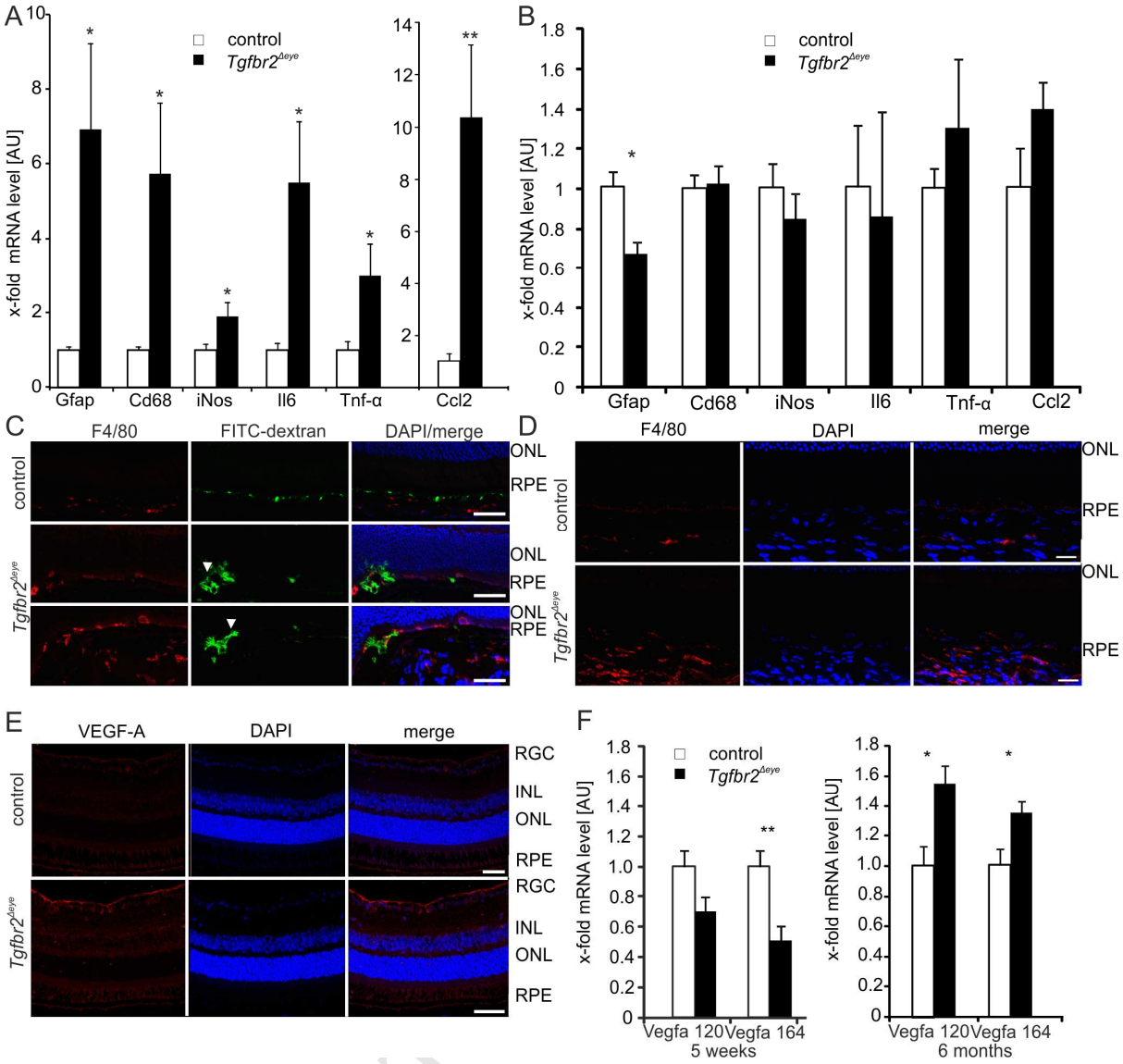
A
control
Tgfbr2Δeye
x-fold mRNA level [AU]
Gfap
Cd68
iNos
Il6
Tnf-α
Ccl2
B
control
Tgfbr2Δeye
x-fold mRNA level [AU]
Gfap
Cd68
iNos
Il6
Tnf-α
Ccl2
C
F4/80
FITC-dextran
DAPI/merge
control
Tgfbr2Δeye
ONL
RPE
D
F4/80
DAPI
merge
control
Tgfbr2Δeye
ONL
RPE
E
VEGF-A
DAPI
merge
control
Tgfbr2Δeye
RGC
INL
ONL
RPE
F
control
Tgfbr2Δeye
x-fold mRNA level [AU]
Vegfa 120
Vegfa 164
5 weeks
Vegfa 120
Vegfa 164
6 months